Ocean Sci. Discuss., 11, 1895–1948, 2014
www.ocean-sci-discuss.net/11/1895/2014/
doi:10.5194/osd-11-1895-2014

Ocean Science
Discussions
Open Access

Deriving a sea surface climatology of CO_2 fugacity in support of air–sea gas flux studies

L. M. Goddijn-Murphy[1], D. K. Woolf[2], P. E. Land[3], J. D. Shutler[3], and C. Donlon[4]

[1]ERI, University of the Highlands and Islands, Ormlie Road, Thurso, UK
[2]ICIT, Heriot-Watt University, Stromness, UK
[3]Plymouth Marine Laboratory, Prospect Place, Plymouth, UK
[4]European Space Agency/ESTEC, Noordwijk, the Netherlands

Received: 27 June 2014 – Accepted: 8 July 2014 – Published: 28 July 2014

Correspondence to: L. M. Goddijn-Murphy (lonneke.goddijn-murphy@uhi.ac.uk)

Published by Copernicus Publications on behalf of the European Geosciences Union.

Abstract

Climatologies, or long-term averages, of essential climate variables are useful for evaluating models and providing a baseline for studying anomalies. The Surface Ocean Carbon Dioxide (CO_2) Atlas (SOCAT) has made millions of global underway sea surface measurements of CO_2 publicly available, all in a uniform format and presented as fugacity, f_{CO_2}. f_{CO_2} is highly sensitive to temperature and the measurements are only valid for the instantaneous sea surface temperature (SST) that is measured concurrent with the in-water CO_2 measurement. To create a climatology of f_{CO_2} data suitable for calculating air–sea CO_2 fluxes it is therefore desirable to calculate f_{CO_2} valid for climate quality SST. This paper presents a method for creating such a climatology. We recomputed SOCAT's f_{CO_2} values for their respective measurement month and year using climate quality SST data from satellite Earth observation and then extrapolated the resulting f_{CO_2} values to reference year 2010. The data were then spatially interpolated onto a $1^\circ \times 1^\circ$ grid of the global oceans to produce 12 monthly f_{CO_2} distributions for 2010. The partial pressure of CO_2 (p_{CO_2}) is also provided for those who prefer to use p_{CO_2}. The CO_2 concentration difference between ocean and atmosphere is the thermodynamic driving force of the air–sea CO_2 flux, and hence the presented f_{CO_2} distributions can be used in air–sea gas flux calculations together with climatologies of other climate variables.

1 Background

1.1 Introduction

Observations demonstrate that dissolved CO_2 concentrations in the surface ocean have been increasing nearly everywhere, roughly following the atmospheric CO_2 increase but with large regional and temporal variability (Takahashi et al., 2009; McKinley et al., 2011). In general, tropical waters release CO_2 to the atmosphere, whereas

OSD
11, 1895–1948, 2014

high-latitude oceans take up CO_2 from the atmosphere. Accurate knowledge of air–sea fluxes of heat, gas and momentum is essential for assessing the ocean's role in climate variability, understanding climate dynamics, and forcing ocean/atmosphere models for predictions from days to centuries (Wanninkhof et al., 2009).

The European Space Agency OceanFlux Greenhouse Gases (GHG) project (http://www.oceanflux-ghg.org/) is an initiative to improve the quantification of air–sea exchanges of greenhouse gases such as CO_2. The project has developed datasets suitable for computation of gas flux climatology in which mean gridded values are computed from multiple measurements over different years. The gas flux calculation requires accurate values of gas transfer velocity, in addition to the concentrations of the dissolved gas above and below the air-water interface (Liss and Merlivat, 1986). The project has relied heavily on the data sets successfully developed and maintained by the Surface Ocean CO_2 Atlas (SOCAT, Bakker et al., 2013; Pfeil et al., 2013; Sabine et al., 2013). SOCAT has collated and carefully quality-controlled the largest collection of ocean CO_2 observations providing data in an agreed and controlled format for scientific activities. Recognising that some groups may have trouble working with millions of measurements, the SOCAT gridded product (Sabine et al., 2013) was then generated to provide a robust, regularly spaced f_{CO_2} product with minimal spatial and temporal interpolation. This gridded climatology is useful for evaluating models and for studying and characterising f_{CO_2} variations within regions in a format that is easy to exploit.

Gas concentrations of CO_2 in the upper ocean can be derived from SOCAT's underway sea surface measurements of fugacity, f_{CO_2} (p_{CO_2} adjusted to account for the fact that the gas is not ideal regarding molecular interactions between the gas and the air). The aquatic CO_2 concentration can be expressed as the product of f_{CO_2} and solubility of CO_2 and the product of CO_2 concentration and gas transfer velocity, k, gives us the air–sea gas flux. Different Authors of CO_2 ocean-atmosphere gas flux products use either a mean value of f_{CO_2} (e.g. Sabine et al., 2013) or p_{CO_2} (e.g. Takahashi 2002, 2009) within a grid box for a particular measurement month and year. Many studies have used the p_{CO_2} climatology of Takahashi et al. (2002, 2009) as a basis to

OSD
11, 1895–1948, 2014

estimate their own air–sea fluxes (e.g., Kettle et al., 2005, 2009; Fangohr and Woolf 2007; Land et al., 2013). The datasets from Takahashi et al. (2002, 2009) and Sabine et al. (2013) are calculated using in situ SST obtained at depth (SST_{depth}) for the construction of ocean CO_2 flux climatology (in situ f_{CO_2} is derived from f_{CO_2} measured in the shipboard equilibrator using the difference between the temperature of sea water in the equilibrator and SST_{depth}). Because f_{CO_2} is highly sensitive to temperature fluctuations, an instantaneous measurement of f_{CO_2} is only really valid for its concurrent in situ SST_{depth} measurement. Takahashi et al. (2009) explain that under-sampling and their interpolation method lead to differences between their p_{CO_2} values with the true climatological mean values. They estimate a mean +0.08 °C temperature difference, introducing a systematic bias of about +1.3 µatm in the mean surface water p_{CO_2} over all monthly mean values obtained in their study. Takahashi et al. (2009) also acknowledge that by using SST_{depth} in their calculations, surface-layer effects could introduce systematic errors in the sea-air p_{CO_2} differences but leave that for future research. Additional SST biases are introduced by different measurement systems that measure SST at sea and that are each associated with typical measurement biases. All biases in SST, and hence in f_{CO_2}, contribute to uncertainties in the true monthly means of f_{CO_2}. A true monthly mean value of f_{CO_2} should therefore be estimated by calculating f_{CO_2} for a monthly mean value of SST; using these values a climatology of f_{CO_2} applicable to air–sea gas flux climatology can then be derived.

The focus of this paper is to critically assess f_{CO_2} calculations and the application of f_{CO_2} for CO_2 ocean gas flux climatology development, in particular the need to properly address the implications of using different SST. We first review the importance of SST on the calculation of f_{CO_2} and the use of satellite SST data. We then review the monthly composite SST data provided by SOCAT and compare those to satellite observations of SST. In Sect. 2 we describe the SOCAT data set and methods, followed by an explanation of our alternative approach to computation of in situ f_{CO_2} to climatological f_{CO_2} (Sect. 3). In Sect. 4 the spatial interpolation using ordinary block kriging is detailed and in Sect. 5 the resulting f_{CO_2} climatology and a range of possible errors

OSD
11, 1895–1948, 2014

are discussed. Our application of the recently released SOCAT version 2 data set is the subject of Sect. 6. In the conclusion (Sect. 7) the different data products and their uses are compared. The month January is used as an illustrative example of the data treatment throughout this paper.

1.2 Complexities of in situ SST measurements and implications for f_{CO_2}

As already discussed, f_{CO_2} is highly sensitive to temperature. Similarly accurate knowledge of SST and, to a lesser extent, salinity, is essential when calculating air–sea gas fluxes. SST vertical profiles are complex and variable. SST can also vary over relatively short time scales within relatively small regions and variations in the temperature measured can also arise from the method and instrumentation used for measuring it. All of these issues can cause problems when using in situ data to construct an f_{CO_2} climatology. These issues are now discussed.

The structure of the upper ocean (~ 10 m) vertical temperature profile depends on the level of shear driven ocean turbulence and the air–sea fluxes of heat, moisture and momentum. Thus, every SST observation depends on the measurement technique and sensor that is used, the vertical position of the measurement within the water column, the local history of all components of the heat flux conditions and, the time of day the measurement was obtained (Donlon et al., 2002). The subsurface SST, SST_{depth} (see Donlon et al., 2007) will encompass any temperature within the water column where turbulent heat transfer processes dominate. Such a measurement may be significantly influenced by local solar heating, the variations of which have a time scale of hours and typically varies with depth. This diurnal warming occurs at the sea surface when incoming shortwave radiation leads to stratification of the surface water in the absence of wind-induced mixing and temperature differences of > 3 K can occur across the surface warm layer (Ward et al., 2004), which in turn will enhance the outgassing flux of CO_2 (Jeffery et al., 2007, 2008; Kettle et al., 2009) that reduces the oceanic carbon uptake (Olsen et al., 2004). Consequently to help address this sort of issue the international Group on High Resolution Sea Surface Temperature (GHRSST)

OSD
11, 1895–1948, 2014

state that SST_{depth} should always be quoted at a specific depth in the water column; e.g., SST_{5m} refers to the SST at a depth of 5 m. However, SST_{depth} data can be measured using a variety of different temperature sensors mounted on buoys, profilers and ships at any depth beneath the water skin and the depth of the measurement is often not recorded. Different measurement systems that are used to measure SST (e.g. hull mounted thermistors, inboard thermosalinograph systems) have evolved over time using different techniques that are prone to different error characteristics (e.g. for a good review see Kennedy, 2013; Kennedy et al., 2011a, b), such as warming of water as it passes through the ships' internal pipes before reaching an inboard thermosalinograph (e.g. Kent et al., 1993; Emery et al., 2001; Reynolds et al., 2010; Kennedy, 2013), poor calibration or biases due to the location and warming of hull mounted temperature sensors (e.g. Emery et al., 1997, 2001), inadequate knowledge of temperature sensor depth (e.g. Emery et al., 1997; Donlon et al., 2007), poor knowledge of temperature sensor calibration performance and local thermal stratification during a diurnal cycle (e.g., Kawai and Wada, 2007). This means that if not carefully controlled, SST biases of > 1 K may easily be introduced into an in situ SST dataset.

All of these issues mean that directly using SST and f_{CO_2} measurement pairs from a large dataset (i.e., that resulting from a large number of different instrument setups and methods) to a f_{CO_2} climatology for studying air–sea gas fluxes is likely to introduce a source of error. Therefore, we propose that correcting all of the f_{CO_2} data back to a consistent surface SST dataset is clearly advantageous and this is where satellite data can provide help.

1.3 The use of satellite sea surface temperature data

Satellite Earth observation thermal infrared radiometers used to sense sea skin temperature variations have been in orbit around the Earth since the 1990s. The resultant data are calibrated to skin temperature (rather than SST at depth) and have been shown to have a higher accuracy and precision for studying SST than in situ methods (e.g., O'Carroll et al., 2008) and such data are now available as a climate data record

OSD
11, 1895–1948, 2014

(Merchant et al., 2008, 2012). We used ARC SST values from the Along Track Scanning Radiometers, ATSRs, Reprocessing for Climate project, ARC, (Merchant et al., 2012). This climate data record is a global, long-term, homogenous, highly stable SST dataset based on satellite derived SST observations.

The difference in the fugacities of CO_2 across the diffusive sub-layer at the ocean surface is the driving force behind the air–sea flux of CO_2. As discussed above in situ sub-surface seawater fugacity is normally measured several meters below the surface. Implied in the use of these measurements for deriving air–sea fluxes is the assumption that the measured fugacity values at depth are the same as those at the bottom of the diffusive boundary layer. Diurnal stratification of the surface ocean further complicates this situation. At wind speeds of approximately $6\,m\,s^{-1}$ and above, the relationship between the SST (at the sea skin) and SST (at depth and below the diffusive sub layer), is well characterized for both day- and night-time conditions by a cool bias (e.g. Donlon et al., 2002). Therefore a skin temperature value from EO with an appropriate correction for the cool skin bias can be used to describe the temperature below the diffusive sub layer. This means that this temperature value can be used to correct the f_{CO_2} from depth to the value below the diffusive sub layer.

1.4 A comparison between SST datasets

In air–sea gas flux calculations an estimate of the water side f_{CO_2}, and hence the temperature, is required at the base of the mass boundary layer. However, ARC SST is measured at the sea surface skin, SST_{skin}, which is characteristically cooler than the water just below it during the night but subject to local diurnal variability and thermal stratification during the day. We derived subskin SST (the SST at the base of the thermal boundary layer) from ARC SST by accounting for the "cool skin effect". Since gas transfer velocities are low in low wind speeds, it is more important to have a reasonably accurate estimate of the thermal skin effect in moderate and high wind speeds. Donlon et al. (1999) reported a mean cool skin ΔT = 0.14 (±0.1) K for wind speeds in excess of $6\,m\,s^{-1}$. We used subskin SST as an

OSD
11, 1895–1948, 2014

approximation of the water temperature in the meters below the surface, SST_{depth} (Donlon et al., 1999; 2002). According to Kettle et al. (2009) the difference between f_{CO_2} for the temperature at the base of the mass boundary layer, and f_{CO_2} for SST_{depth} is negligible so we calculated f_{CO_2} using subskin SST to estimate f_{CO_2} at the base of the mass boundary layer. The ARC dataset provides SST_{skin} from infrared imagery gridded to a 0.1° latitude–longitude resolution (Merchant et al., 2012). For each year from August 1991 to December 2010 Oceanflux GHG derived 12 monthly mean SST_{skin} distributions, averaged over a $1^\circ \times 1^\circ$ grid without differentiating between day- and night-time measurements (http://www.oceanflux-ghg.org/Products/OceanFlux-data/Monthly-composite-datasets). These SST_{skin} grid points were linearly interpolated to the SOCAT measurement locations ($SST_{skin,i}$). We defined T_{ym} as the single year, monthly $1^\circ \times 1^\circ$ grid box mean of $T_{ym,i} = SST_{skin,i} + 0.14$. The f_{CO_2} values were re-computed from in situ SST to $T_{ym,i}$ for our climatology (Sect. 3.2).

With SST the corresponding grid box mean of SOCAT's in situ SST (generally obtained at 5 m nominal depth) and using all data from the years 1991 to 2007, a histogram of $dT = T_{ym} - SST$ was produced (Fig. 1). It shows dT was distributed around a mean of −0.09 with a standard deviation of 0.55. This difference implied that the gridded in situ SST systematically overestimated T_{ym}. The corresponding histogram of our correction $f_{CO_2}(T_{ym}) - f_{CO_2}$ (SST) (not shown) revealed a similar distribution around −1.12 µatm. The temperature differences were found to be positive as well as negative (Fig. 1). Positive dT can be a consequence of diurnal warming when the top layer heats up by solar radiation during the day. This heat is lost again during the night. Cooling of the top layer (negative dT) is a less described phenomenon but can be expected in colder environments. We found more negative dT during the winter months and at high latitudes. The temperature profile in the sea depends on wind speed as wind mixes the water column, i.e. for strong winds SST is expected to be more constant in the vertical. We illustrate the wind speed dependence of dT for the North Atlantic because this region has the highest SOCAT data density. For each dT we retrieved the monthly $1^\circ \times 1^\circ$ grid box mean of 10 m wind speed, U_{10} ($m\,s^{-1}$), from Oceanflux

OSD
11, 1895–1948, 2014

GHG's composite of GlobWave merged altimeter data (http://www.oceanflux-ghg.org/Products/OceanFlux-data/Monthly-composite-datasets). A scatter plot of dT as a function of U_{10}, averaged over in 1 m s^{-1} U_{10} bins, (Fig. 2) showed that dT decreased with increasing U_{10} becoming negative for wind speeds over about 10 m s^{-1}. Similar trends were seen in the other regions, but with dT turning negative for different wind speeds: North Pacific 9 m s^{-1}; Coastal 8 m s^{-1}; Tropical Atlantic and Southern Ocean 6 m s^{-1}; Tropical Pacific, Indian Ocean and Arctic 4 m s^{-1} (SST data from Bakker et al., 2013). The Tropical Atlantic was different in that dT became less negative for wind speed over ~ 8 m s^{-1}, turning positive over ~ 10 m s^{-1}. If only North Atlantic data from the winter months December, January and February were included, nearly all dT values would be negative.

1.5 The OceanFlux climatology of f_{CO_2} and SST

We have converted the SOCAT's instantaneous f_{CO_2} (and SST) data to a monthly mean f_{CO_2} using a climate data record of SST. This approach has only recently become possible due to the availability of the consistently calibrated sea surface temperature climate record (Merchant, 2008, 2012). In order to eliminate biases due to the sampling year (i.e., surface ocean f_{CO_2} has been increasing over the years) f_{CO_2} values from all years were extrapolated to reference year 2010 using a simple linear relationship.

2 The SOCAT database

2.1 Introduction

The SOCAT database contains millions of surface ocean CO_2 measurements in all ocean areas spanning four decades. All data are put in a uniform format while clearly defined criteria are applied in their quality control. SOCAT has been made possible through the cooperation (data collection and quality control) of the international marine

OSD
11, 1895–1948, 2014

carbon science community. The history and organisation of SOCAT is described in Pfeil et al. (2013). SOCAT version 1.5 includes 6.3 million measurements from 1968 to 2007 and was made publicly available in September 2011 at http://www.socat.info/SOCATv1/ . SOCAT data is available as three types of data products: individual cruise files, gridded products and merged synthesis data files. For our study we used the latter and we downloaded the individual regional synthesis files from http://cdiac.ornl.gov/ftp/oceans/SOCATv1.5/. The content of these files (parameter names, units and descriptions) are described in Table 5 in Pfeil et al. (2013). The data can be displayed in the online Cruise Data Viewer (Fig. 3) and downloaded in text format.

2.2 The SOCAT computation of SOCAT fugacity in seawater

The collected CO_2 concentrations are expressed as mole fraction, x_{CO_2}, partial pressure, p_{CO_2}, or fugacity, f_{CO_2}, of CO_2. SOCAT's re-computation is to achieve a uniform representation of the CO_2 measurements and all measurements are converted to fugacity in seawater $f_{CO_2,is}$ (fCO2_rec) for in situ sea surface, SST (temp). The parameters in brackets refer to their SOCAT version 1.5 names (Table 5 in Pfeil et al., 2013). SST is the intake temperature which signifies SST_{depth}. The shipboard measurements were taken at equilibrator temperature T_{eq} (Temperature_equi) and equilibrator pressure, P_{eq} (Pressure_equi). SOCAT calculates $f_{CO_2,is}$ from $p_{CO_2,is}$, partial pressure in seawater corrected for the difference between SST and the temperature at the equilibrator, using Eqs. (1) and (2)

$$p_{CO_2,is} = p_{CO_2}(T_{eq}) \exp(0.0423(SST - T_{eq})) \quad (1)$$

$$f_{CO_2,is} = p_{CO_2,is} \exp\left(\frac{\left[B(CO_2, SST) + 2(1 - x_{CO_2,wet}(T_{eq}))^2 \delta(CO_2, SST)\right] P_{eq}}{R \cdot SST}\right) \quad (2)$$

OSD
11, 1895–1948, 2014

with $B(CO_2, SST)$ and $\delta(CO_2, SST)$ calculated from Weiss (1974):

$$B(CO_2,T) = -1636.75 + 12.0408T - 3.27957 \times 10^{-2}T^2 + 3.16528 \times 10^{-5}T^3 \quad (3)$$

$$\delta(CO_2,T) = 57.7 - 0.118T \quad (4)$$

(Pfeil and Olsen, 2009). In Eqs. (1)–(4) f_{CO_2} and p_{CO_2} are in µatm, P_{eq} in hPa, temperatures are in kelvins and $x_{CO_2,wet}(T_{eq})$ is the wet mole fraction as parts per million (ppm) of CO_2 at equilibrator. The gas constant $R = 82.0578\,cm^3\,atm\,(mol\,K)^{-1}$. How $p_{CO_2}(T_{eq})$ is measured, the temperature correction (Eq. 1) and the necessarily different starting points of the computation are discussed in respective Sects. 2.3–2.5. Our conversion, from the given $f_{CO_2,is}$ calculated for in situ measurements to climatological $f_{CO_2,cl}$ in 2010 is explained in Sect. 3.

2.3 Measurements of $p_{CO_2}(T_{eq})$

The measurement method of p_{CO_2} in seawater described by Takahashi et al. (2009) is summarized in the following. On board the ship carrier gas is equilibrated with streaming seawater in the headspace of an equilibrator and the concentration of CO_2 in the equilibrated carrier gas is measured. When a dry carrier gas is analysed, seawater $p_{CO_2}(T_{eq})$ in the equilibrator chamber is computed using

$$p_{CO_2}(T_{eq}) = x_{CO_2,dry}(P_{eq} - P_w) \quad (5)$$

where P_{eq} is the pressure at the equilibrator, P_w water vapour pressure at T_{eq} and salinity (S), and $x_{CO_2,dry}$ the mole fraction of CO_2 in dry air. P_w is calculated with

$$P_w = \exp(24.4543 - 67.4509(100/T_{eq}) - 4.8489(\ln(T_{eq}/100) - 0.000544S) \quad (6)$$

with T_{eq} in Kelvin and S the sample salinity (Pfeil and Olsen, 2009). When mixing ratios in a wet carrier gas (100 % humidity) are determined, P_w is set to zero

$$p_{CO_2}(T_{eq}) = x_{CO_2,wet}P_{eq}. \quad (7)$$

OSD
11, 1895–1948, 2014

2.4 Temperature handling

There are different methods to correct for the difference in partial pressure at intake and equilibrator temperature. SOCAT uses the simple Eq. (1) (Pfeil and Olsen, 2009); they refer to more complicated methods but disregard these because they require knowledge of the total dissolved inorganic carbon, T_{CO_2}, and alkalinity, T_{Alk}, and are not determined for isochemical conditions. Takahashi et al. (2009) use

$$p_{CO_2,is} = p_{CO_2}(T_{eq}) \exp\left(0.0433(SST - T_{eq}) - 4.35 \times 10^{-5}\left(SST^2 - T_{eq}^2\right)\right) \quad (8)$$

with SST and T_{eq} in °C. Equations (1) and (8) correct for the effect of slight warming before measurement at the equilibrator on an isochemical transformation (T_{CO_2} and T_{Alk} are unchanged but pH and aqueous CO_2 concentration may vary). Equation (8) is an integrated form of

$$\delta \ln(p_{CO_2})/\delta T = 0.0433 - 8.7 \times 10^{-5} T$$

while in Eq. (1) a mean coefficient of $0.0423\,°C^{-1}$ is used. Equation (8) was therefore expected to give more accurate $p_{CO_2,is}$ estimates.

2.5 Starting points of the SOCAT computation

Different measured parameters are available in different records to use as starting point for the SOCAT re-computation of $f_{CO_2,is}$ (Table 4 in Pfeil et al., 2013). Therefore SOCAT applies the following strict guidelines:

1. recalculate f_{CO_2} whenever possible;
2. order of preference of the starting point is: x_{CO_2}, p_{CO_2}, f_{CO_2};
3. minimize the use of external data.

OSD
11, 1895–1948, 2014

The majority of the cases (57.5 %) is derived from $x_{CO_2,dry}(T_{eq})$. However, in many cases only $f_{CO_2,is}$ (8.4 %) or $p_{CO_2,is}$ (13.8 %) was provided so that it is not certain that Eq. (1) was used by the cruise scientists to convert $p_{CO_2}(T_{eq})$ to $p_{CO_2,is}$. Moreover, if only $f_{CO_2,is}$ was reported, but pressure and salinity were not, $f_{CO_2,is}$ is not recalculated and $f_{CO_2,is}$ is taken as provided. The regional synthesis files only contain re-computed $f_{CO_2,is}$ values and don't give direct information about starting points other than which one was used (fCO2_source). However, each record contains a field "doi", indicating the digital object identifier to a publically accessible online data file in the PANGAEA database (http://www.pangaea.de/) where the original measurements before re-computation can be found. The individual cruise data files also contain various x_{CO_2}, p_{CO_2}, and f_{CO_2} data (Table 5 in Pfeil et al., 2013). Because we wanted to use SOCAT's uniform database, and not re-create it, we estimated $f_{CO_2,cl}$ from the $f_{CO_2,is}$ values in the merged synthesis files as explained in Sect. 3. An estimation of the errors in re-computed $f_{CO_2,cl}$ due to varying starting points is given in Sects. 5.6 and 5.7.

3 Our re-computation for climatological fugacity in the year 2010

3.1 Inversion: conversion of $f_{CO_2,is}$ to $p_{CO_2}(T_{eq})$

We used Eqs. (2) and (8) (with SST = $T_{ym,i}$) to calculate $f_{CO_2,ym,i}$ but because mole fraction $x_{CO_2,is}$, and partial pressures $p_{CO_2,is}$ and $p_{CO_2}(T_{eq})$ are not given in the SOCAT regional synthesis files, the first step was to estimate the original measurement of $p_{CO_2}(T_{eq})$. First $p_{CO_2,is}$ was derived from $f_{CO_2,is}$ by inverting Eq. (2):

$$p_{CO_2,is} = f_{CO_2,is} \exp\left(-\frac{\left[B + 2(1 - x_{CO_2,wet}(T_{eq}))^2 \delta\right] P_{eq}}{R \cdot \text{SST}}\right) \quad (9)$$

with $B = B(CO_2, \text{SST})$ and $\delta = \delta(CO_2, \text{SST})$ from Eqs. (3) and (4) and SST the SOCAT measurement. Defining $x_{CO_2,wet}(T_{eq})$ as $p_{CO_2}(T_{eq})/P_{eq}$ (Eq. 7) and writing $p_{CO_2}(T_{eq})$ in

OSD
11, 1895–1948, 2014

terms of $p_{CO_2,is}$ (Eq. 1), Eq. (9) leads to

$$p_{CO_2,is} = f_{CO_2,is} \exp\left(-\frac{\left[B + 2\left(1 - \frac{p_{CO_2,is}\exp(-0.0423(SST - T_{eq}))}{P_{eq}}\right)^2 \delta \right] P_{eq}}{R \cdot SST} \right). \quad (10)$$

Equation (10) was solved with an iterative calculation

$$[p_{CO_2,is}]_{n+1} = f_{CO_2,is} \exp(g([p_{CO_2,is}]_n, SST, T_{eq}, P_{eq})) \quad (11)$$

(with g a function describing the exponent). In the first iteration the initial guess of $[p_{CO_2,is}]_1$ was $f_{CO_2,is}$ and the result $[p_{CO_2,is}]_2$ was put back in the right hand side of Eq. (11). This step was repeated until $|[p_{CO_2,is}]_N - [p_{CO_2,is}]_{N-1}| < 2^{-52}$. Using Eq. (1) we could then estimate the original $p_{CO_2}(T_{eq})$,

$$p_{CO_2}(T_{eq}) = p_{CO_2,is} \exp(-0.0423(SST - T_{eq})) \quad (12)$$

3.2 Conversion of $p_{CO_2}(T_{eq})$ to $f_{CO_2,cl}$ in the year 2010

The next step was to convert partial pressure at equilibrator temperature to partial pressure at $T_{ym,i}$ for each SOCAT measurement. Because ARC ATSR data were available from August 1991 we converted SOCAT data from then onwards. As a consequence 95 249 (1.4 %) of valid f_{CO_2} observations were not used from the SOCAT v1.5 dataset (from 119 cruises spread all over the globe). We note that the ESA CCI project is now working on an extended SST climate data record from satellite extending back to 1981 which is expected in 2015. Following Takahashi et al. (2009) we used Eq. (8) to correct for the difference between climatological and equilibrator temperature

$$p_{CO_2,ym,i} = p_{CO_2}(T_{eq}) \exp\left(0.0433(T_{ym,i} - T_{eq}) - 4.35 \times 10^{-5}\left(T_{ym,i}^2 - T_{eq}^2\right)\right) \quad (13)$$

OSD
11, 1895–1948, 2014

The subscript "ym" indicates a "single year monthly composite" and "i" interpolated to SOCAT sample location (Sect. 1.4). Equation (8) was applied because an isochemical transformation between SST and T_{ym} was a reasonable assumption, i.e. total carbon and alkalinity in the ocean surface was not expected to vary significantly during one month. Next, monthly composite estimations of $f_{CO_2,ym,i}$ were calculated from $p_{CO_2,ym,i}$ according to Eq. (2),

$$f_{CO_2,ym,i} = p_{CO_2,ym,i} \exp\left(\frac{\left[B + 2\left(1 - \frac{p_{CO_2}(T_{eq})}{P_{eq,ym}}\right)^2 \delta\right] P_{eq,ym}}{R \cdot T_{ym,i}}\right) \quad (14)$$

with $B = B(CO_2, T_{ym,i})$ (Eq. 3) and $\delta = \delta(CO_2, T_{ym,i})$ (Eq. 4). We estimated $P_{eq,ym}$ from sea level pressure estimated at closest grid value from 6 hourly NCEP/NCAR as given in SOCAT's merged synthesis files (ncep_slp). To account for the overpressure that is normally maintained inside a ship 3 hPa was added ($P_{eq,ym}$ = ncep_slp + 3 hPa) (Takahashi et al., 2009). Note that we recomputed SOCAT's f_{CO_2} for monthly composite SST and atmospheric pressure, but not for monthly composite salinity. However, if in situ salinity was not provided by the investigator, SOCAT used a monthly composite sea surface salinity from the World Ocean Atlas 2005 (woa_sss) for their computation of $f_{CO_2,is}$. The consequences of missing salinity values are assessed in Sect. 5.7. For all years $p_{CO_2,ym,i}$ and $f_{CO_2,ym,i}$ were extrapolated to the year 2010, producing $p_{CO_2,cl,i}$ and $f_{CO_2,cl,i}$ referenced to 2010, using the same mean rate of change (1.5 ± 0.3 µatm yr^{-1}) as Takahashi et al. (2009) used for p_{CO_2}. Takahashi et al. (2009) extrapolate to the year 2000, so if the rate of change has increased since then ours could be a low estimate. Finally, the $f_{CO_2,cl,i}$ and $p_{CO_2,cl,i}$ data were grouped by month and averaged over 1° × 1° squares. Not all 1° × 1° grid boxes were filled and we horizontally interpolated between filled values to produce global $p_{CO_2,cl}$ and $f_{CO_2,cl}$ distributions (Sect. 4).

OSD
11, 1895–1948, 2014

3.3 Missing values

We dealt with missing SOCAT variables following Pfeil and Olsen (2009):

1. we only used "good" records (WOCE_flag = 2);
2. we only used records with valid $f_{CO_2,is}$ and SST;
3. if T_{eq} was invalid we used SST;
4. if P_{eq} was invalid we used atmospheric pressure, P_{atm}, +3 hPa;
5. if P_{eq} and P_{atm} were invalid we used ncep_slp + 3 hPa.

4 Horizontal extrapolation using ordinary block kriging

Unlike Takahashi et al. (2009), our climatology includes data from El Niño years and coastal locations. We added $p_{CO_2,cl}$ for those who prefer to use partial pressure; $p_{CO_2,cl}$ levels were slightly higher (less than 2 µatm) than $f_{CO_2,cl}$. For the spatial interpolation of the gridded data on a 1° × 1° mask map of the global oceans we used gstat, an open source computer code for multivariable geostatistical modelling, prediction and simulation (gstat home page: http://www.gstat.org/). Gstat finds the best linear unbiased prediction (the expected value) with its prediction error for a variable at a location, given observations and a model for their spatial variation (Pebesma, 1999). We quantified the prediction error as standard deviation (square root of the variance given by gstat). First, we modelled the variogram for $f_{CO_2,cl}$ for each month using gstat's interactive user interface (Pebesma, 1999). A variogram describes how the data varies spatially and can be represented by a plot of semivariance against distance. The variograms best fitted combinations of a nugget and a spherical model, a Nug(0) + b Sph(c), and for each month variogram parameters a, b and c were derived (e.g., Fig. 4). The fitted variogram models were applied in the kriging of both $f_{CO_2,cl}$ and $p_{CO_2,cl}$. For $p_{CO_2,cl}$ we

OSD
11, 1895–1948, 2014

used the same variogram as for $f_{CO_2,cl}$ because the difference with $f_{CO_2,cl}$ was negligible compared to the spatial variation.

We applied ordinary kriging on mask map locations because it is the default action when observations, variogram, and prediction locations are specified (Pebesma, 1999). We performed local ordinary block kriging on a $1^\circ \times 1^\circ$ mask map of the global oceans with min = 4, max = 20, and radius = 60. Thus, after selecting all data points at (euclidian) distances from the prediction location less or equal to 60, the 20 closest were chosen when more than 20 were found and a missing value was generated if less than 4 points were found. The data were smoothed by averaging over square shaped 5×5 sized blocks. Thus gstat produced the $f_{CO_2,cl}$ (and $p_{CO_2,cl}$) prediction and variance values located at the grid cell centres of the (non-missing valued) cells in the grid map mask. These results were compared with results from different kriging options min, max, radius and block size (Sect. 5.3).

Our approach was simpler than the spatial interpolation on a $4^\circ \times 5^\circ$ grid of Takahashi et al. (2009). For each day they increase pixel size to four neighbouring pixels over 3 days (past, present and future day). The values of the pixels that are still without observations after this procedure are computed by a continuity equation based on a 2-D diffusion–advection transport equation for surface waters. All daily pixel values are used to calculate monthly mean values. Takahashi et al. (2009) estimate that the global mean surface water $p_{CO_2,cl}$ obtained in their study may be biased by about +1.3 µatm due to under sampling and the interpolation method. The spatial interpolation method we applied is expected to give unbiased results (Pebesma, 1999).

5 Results

5.1 Monthly global maps

The prediction distributions of $f_{CO_2,cl}$ produced by the ordinary block kriging are shown in Fig. 5 for all 12 months. The maps showing the standard deviations of the kriging

OSD
11, 1895–1948, 2014

for January (all months) are show in Fig. 6 (Fig. A1). The 12 monthly global distribution data have been made available in 12 netCDF-3 files in the Supplement related to this article. These files contain $f_{CO_2,cl}$, $p_{CO_2,cl}$, their spatial interpolation errors, and ARC's SST_{skin} for the year 2010, all on a $1^\circ \times 1^\circ$ grid. The variable names are respectively fCO2_2010_krig_pred, pCO2_2010_krig_pred, fCO2_2010_krig_std, pCO2_2010_krig_std, and Tcl_2010 (T_{ym} as defined in Sect. 1.4 for the year 2010). Monthly gridded values of atmospheric CO_2 dry air mole fractions in 2010, made available by the NOAA ESRL Carbon Cycle Cooperative Global Air Sampling Network (Dlugokencky et al., 2014), are also given as variable vCO2_2010. These were not used in our conversion but can help calculate air-sea gas CO_2 fluxes (Takahashi, 2009). The important differences with the Takahashi climatology are summarized in Table 1.

A range of errors needs to be considered when interpreting the final monthly maps. It is difficult to be complete but we considered the following errors. The spatial interpolation errors were estimated by taking the square root of the variances of the kriging. The different kriging approaches themselves were evaluated by calculating the mean and standard deviations of the varying $f_{CO_2,cl}$ kriging results using the options shown in Table 2. The cruises were bootstrapped to investigate if certain cruises dominated the mapped results. Other errors that were analysed were the "temporal extrapolation error", the "inversion error" related to the different starting points, the consequences of the missing values, and the propagations of the uncertainties in the SOCAT measurements and $T_{ym,i}$. These errors are discussed in the next sub sections and the final sub section gives a summary overview.

5.2 Spatial interpolation errors

The standard deviations (SD) of the applied kriging were calculated by taking the square root of the variance values produced by gstat (Pebesma, 1999). Kriging errors were obviously related to the available SOCAT data density in the measurement month (e.g., Fig. 3). The $f_{CO_2,cl}$ kriging SD mapped for all months are illustrated in Fig. A1. The monthly SD over all grid points was 20 ± 5 µatm on average (mean over all monthly

OSD
11, 1895–1948, 2014

means ± Sd). The average monthly minimum and maximum SD values were 6.3 ± 2.6 and 50 ± 8.7 µatm. Problem areas emerged where no SOCAT data were available, for example in the western Southern Ocean and the Arctic. Spatial interpolation errors were lowest in the North Atlantic and North Pacific where SOCAT data was dense. The month April showed the highest errors, this could be a consequence of the variogram range, c, being the smallest (implying that the covariance between the locations dropped quickly with distance). Our variogram model of combination of a nugget and a spherical model did not fit November data well as the semivariance was almost independent of distance; the low standard deviations in November (Fig. A1) were therefore probably not representative of the true error due to the kriging method. Standard deviations of the kriging are included in our presented data files; a bias is not supposed to be introduced by the kriging itself (Pebesma, 1999).

5.3 A comparison of the different kriging approaches

The ordinary block kriging of the $f_{CO_2,cl}$ data was repeated using a range of sensible kriging parameters (Table 2). The standard deviation of the mean over the different kriging results (Figs. 7 and A2) was less than 5 µatm in most places, with higher values seen near the coasts, Arctic, and the western Tropical Pacific and Southern Ocean. These standard deviations were considerably smaller than those of the kriging itself (Figs. 6 and A1) but could be significant in a few places especially, but not exclusively, in the Arctic and coastal regions.

5.4 Are some cruises more important than others?

It was conceivable that certain cruises dominated the final results. This possibility was studied using the bootstrap method, a statistical technique which permits the assessment of variability in an estimate using just the available data (Wilmott et al., 1985). Bootstrapping creates synthetic sets of data by random resampling from the original data with replacement. We bootstrapped the SOCAT data 10 times by cruise ID to

OSD
11, 1895–1948, 2014

estimate the variability of the mean monthly $f_{CO_2,cl}$ distributions. The complete SOCAT data set was too big to bootstrap at once. We therefore bootstrapped in two steps, first by cruise ID for each year and region, and then by year and region. Each of the 10 resulting $f_{CO_2,cl}$ datasets were kriged as described in Sect. 4 (for each month in each synthetic dataset a different variogram model was fitted and applied). The mean monthly distributions showed that in regions of fewer cruises (outside the North Atlantic and North Pacific) significant variation in $f_{CO_2,cl}$, could occur, with up to 50 µatm standard deviation (Figs. 8 and A3). It was therefore likely that certain cruises were indeed more important than others. High variability in the east-central equatorial Pacific could be a consequence of not excluding the El Nino years.

5.5 Temporal extrapolation error

The 1.5 µatm yr^{-1} rate of change in p_{CO_2} has an estimated precision of ±0.3 µatm yr^{-1} (Takahashi et al., 2009) and $\Delta f_{CO_2,cl} = \Delta p_{CO_2,cl}$ (Eq. 14). The error in $f_{CO_2,cl}$ in 2010 due to uncertainty of the $p_{CO_2,cl}$ trend was therefore estimated as $\pm(2010 - \text{year}) \cdot 0.3\,\mu\text{atm}\,yr^{-1}$, ranging between ±(0.9–5.7) µatm. These extrapolation errors for the month of January and for all months are shown in respective Fig. 9 and Fig. A4. The error was on the high side in the Indian Ocean and in the western Southern Ocean because fewer cruises were performed there in recent times. The absolute monthly mean extrapolation error over all grid points was estimated at 3 ± 0.1 µatm (average over all monthly means ± standard deviation). This implies that if in reality the rate of change since 1991 was 1.8 instead of 1.5 µatm yr^{-1}, $f_{CO_2,cl}$ would be underestimated by ∼ 3 µatm on average. Recent research has shown that this is probable, as Takahashi et al. (2014) present an updated oceanic p_{CO_2} trend of 1.9 µatm yr^{-1}, a value supported by McKinley et al. (2011).

OSD
11, 1895–1948, 2014

5.6 Inversion error

Our conversion of $f_{CO_2,is}$ to $p_{CO_2}(T_{eq})$ could introduce an error if the data was not based on x_{CO_2} analysis (cruise flags not A or B), but on f_{CO_2} calculated from a spectrophotometer, or if the investigator only provided $f_{CO_2,is}$ or $p_{CO_2,is}$ and did not use Eq. (1) to correct for the temperature difference. This error was assessed by calculating the conversion from $f_{CO_2,is}$ to $f_{CO_2,ym,i}$ using SST and P_{eq} instead of T_{ym} and $P_{eq,ym}$. This conversion would ideally produce the original SOCAT $f_{CO_2,is}$ value. A difference between $f_{CO_2,is}$ and "$f_{CO_2,ym,i=is}$" implied that our re-computation differed from the one applied by SOCAT or the investigator and we called this difference averaged over one grid box "inversion error". Note that $\Delta f_{CO_2,cl} = \Delta f_{CO_2,ym}$. This error turned out in a very small positive bias, negligible in the North Atlantic and other areas with some higher levels in the Southern Ocean (Figs. 10 and A5). The monthly mean inversion bias over all grid points was 1 ± 0.2 µatm (average over all monthly means ± standard deviation).

5.7 Missing values

A related problem was introduced by missing SOCAT values (Sect. 3.3). Missing values did not always propagate into an inversion error because we made an effort to handle the missing values following SOCAT (Pfeil and Olsen, 2009). If salinity or pressure were missing, SOCAT used EO values for their conversion, reducing systematic $f_{CO_2,cl}$ errors in our re-conversion. Missing values of temperature and pressure at the equilibrator could introduce systematic errors, however. It is difficult to estimate the size of these kinds of errors, but Fig. 11 shows the proportion of missing values for January to give an idea about how many data could be affected. The $f_{CO_2,ym,i}$ calculations were most sensitive to temperature. If T_{eq} was not provided we used in situ SST, so an inversion error would be near zero. However, in these cases $p_{CO_2,is}$ was then the starting point of our conversion instead of $p_{CO_2}(T_{eq})$ which could lead to significant systematic $f_{CO_2,ym,i}$ errors. We therefore also reproduced our $f_{CO_2,cl}$ distribution maps using only data points with valid T_{eq} values (Figs. 12 and A6). These maps appeared to reveal

OSD
11, 1895–1948, 2014

less high $f_{CO_2,cl}$ outliers. If only data with valid T_{eq} were selected the data quality was believed to be better, but the number of data points was compromised. The monthly distributions of these data (Fig. A7) therefore showed either lower or higher SD levels. The monthly mean difference $f_{CO_2,cl}(\text{all}) - f_{CO_2,cl}(\text{valid}\, T_{eq})$ ranged between −3.3 µatm (November) and 3.7 µatm (January) and was −0.4 µatm on average. The error due to missing values in a monthly distribution file could therefore be interpreted as smaller than about ±3.5 µatm, resulting in a bias of the annual mean of −0.4 µatm.

5.8 Measurement errors

Errors in the SOCAT measurements ($f_{CO_2,is}$, T_{eq}, P_{eq} and SST) naturally propagated into $f_{CO_2,cl}$ uncertainty. The accuracies for the SOCAT measurements that comply with SOP (Standard Operating Procedures) criteria are given by Pfeil et al. (2013); not all SOCAT data are of this high standard so these accuracies were the highest that could be expected. Likewise the uncertainty in $T_{ym,i}$ had to be taken into account. Ocean-flux GHG gives the SD values and counts with the mean SST_{skin} values from ARC on a 1° × 1°grid; the average standard error ($SD/\sqrt{count}$) over all monthly grid boxes that had f_{CO_2} values (all years and months) was ±0.17. The uncertainty in the SST difference with subskin SST is ±0.1 (Donlon et al., 1999). The total uncertainty in $T_{ym,i}$ was therefore estimated to be ±0.2 ($\sqrt{0.17^2 + 0.1^2}$). We estimated the propagation of these errors by applying the error for each parameter, x, and calculate $f_{CO_2,cl}$. (We calculated $f_{CO_2,cl}$ for $x + \Delta x$ and $x - \Delta x$ and $\Delta f_{CO_2,cl} =$ mean $\{(f_{CO_2,cl}(x + \Delta x) - f_{CO_2,cl}(x - \Delta x))/2\}$. The results are listed in Table 3. The total error caused by known uncertainties in the parameters was estimated to be > 3.7 µatm ($\sqrt{0.75^2 + 0.015^2 + 2^2 + 3^2}$).

5.9 Summary of errors

The standard deviations of the kriging should account for both spatial variation of the data points and random errors in the $f_{CO_2,cl}$ values. The errors caused by the

OSD
11, 1895–1948, 2014

uncertainty of the rate of p_{CO_2} change (temporal extrapolation error), missing values and measurement errors are of the latter kind. Their monthly averages were estimated at 3, 3.5 and 3.7 µatm respectively and hence we could explain 5.9 µatm ($\sqrt{3^2 + 3.5^2 + 3.7^2}$) of the about 20 µatm monthly average SD of the fit. Note that an error of 5.9 µatm agrees well with the average monthly minimum SD of the kriging of 6.3 ± 2.6 µatm, leaving some room for unexplained errors (Sect. 5.2). The above analysis shows that the SD of the kriging was dominated by the spatial variation of the data, closely linked to data density.

We estimated a bias of ~ 1 µatm, introduced by the inversion step in the $f_{CO_2,is}$ to $f_{CO_2,ym,i}$ conversion. The mean $f_{CO_2,cl}$ over all months had a bias of −0.4 µatm due to missing SOCAT values in the re-computation, so for the total bias of an annual average $f_{CO_2,cl}$ we estimated a value between 0.6 and 1 µatm. This is less than the systematic bias in the mean surface water p_{CO_2} of about 1.3 µatm as estimated by Takahashi et al. (2009) due to under sampling and their interpolation. If we also account for a 3 µatm underestimation of the oceanic p_{CO_2} trend, the bias would range between −2.4 and −2 µatm.

6 SOCAT version 2

Recently, on 4 June 2013, the updated database SOCAT version 2 was released containing 10.1 million surface water f_{CO_2} values (Bakker et al., 2013). The added data are from cruises during the years 2008 to 2011, from the Arctic, and previously unpublished data from earlier cruises; also the quality control is improved. The addition of SOCAT data points and the omission of bad and questionable data gave smoother global distributions (Fig. 13) and smaller kriging errors (Fig. A8). The monthly average of the SD of the kriging was 17 ± 3 µatm (was 20 ± 5 µatm for version 1.5). The monthly mean difference $f_{CO_2,cl}$ (v1.5) – $f_{CO_2,cl}$(v2) ranged between −1.1 µatm (January) and 2.4 µatm (July) and was 0.3 µatm on average. Our re-processed SOCAT version 2 data has also been made available.

OSD
11, 1895–1948, 2014

7 Conclusions

SOCAT f_{CO_2} (and p_{CO_2}) predictions and standard deviations for a reference year 2010, recomputed for a SST suitable for climate change research of air–sea gas exchange and interpolated to a global $1^\circ \times 1^\circ$ grid, have been made available. Two climatology datasets are presented as an online Supplement to this paper, each consisting of 12 monthly NetCDF files: one using all SOCATv1.5 data and one using all data of the recent update SOCATv2. We identified and calculated various possible errors. The errors due to the spatial interpolation, closely related to data density, dominated and some areas showed higher errors of all kinds than others. The data quality/density in the North Atlantic and North Pacific proved to be superior. Our dataset based on SOCAT version 2 is mostly similar to the one based on version 1.5, but if it is used to focus on outliers version 2 should be used because the data quality is better. For future SOCAT versions: it would benefit climatological applications if additional climatological values of f_{CO_2} were directly calculated using the difference between the temperature of sea water in the equilibrator and monthly composite temperatures such as from ARC (Eq. 13), so to avoid the inversion step.

The Supplement related to this article is available online at doi:10.5194/osd-11-1895-2014-supplement.

Acknowledgements. This research is a contribution of the National Centre for Earth Observation, a NERC Collaborative Centre and was supported by the European Space Agency (ESA) Support to Science Element (STSE) project OceanFlux Greenhouse Gases (contract number: 4000104762/11/I-AM). We appreciate the use of the SOCAT data, made available by SOCAT investigators, regional group leaders, quality controllers and data providers.

OSD
11, 1895–1948, 2014

References

Bakker, D. C. E., Pfeil, B., Smith, K., Hankin, S., Olsen, A., Alin, S. R., Cosca, C., Harasawa, S., Kozyr, A., Nojiri, Y., O'Brien, K. M., Schuster, U., Telszewski, M., Tilbrook, B., Wada, C., Akl, J., Barbero, L., Bates, N. R., Boutin, J., Bozec, Y., Cai, W.-J., Castle, R. D., Chavez, F. P., Chen, L., Chierici, M., Currie, K., de Baar, H. J. W., Evans, W., Feely, R. A., Fransson, A., Gao, Z., Hales, B., Hardman-Mountford, N. J., Hoppema, M., Huang, W.-J., Hunt, C. W., Huss, B., Ichikawa, T., Johannessen, T., Jones, E. M., Jones, S. D., Jutterström, S., Kitidis, V., Körtzinger, A., Landschützer, P., Lauvset, S. K., Lefèvre, N., Manke, A. B., Mathis, J. T., Merlivat, L., Metzl, N., Murata, A., Newberger, T., Omar, A. M., Ono, T., Park, G.-H., Paterson, K., Pierrot, D., Ríos, A. F., Sabine, C. L., Saito, S., Salisbury, J., Sarma, V. V. S. S., Schlitzer, R., Sieger, R., Skjelvan, I., Steinhoff, T., Sullivan, K. F., Sun, H., Sutton, A. J., Suzuki, T., Sweeney, C., Takahashi, T., Tjiputra, J., Tsurushima, N., van Heuven, S. M. A. C., Vandemark, D., Vlahos, P., Wallace, D. W. R., Wanninkhof, R., and Watson, A. J.: An update to the Surface Ocean CO_2 Atlas (SOCAT version 2), Earth Syst. Sci. Data, 6, 69–90, doi:10.5194/essd-6-69-2014, 2014.

Dlugokencky, E. J., Masarie, K. A., Lang, P. M., and Tans, P. P.: NOAA Greenhouse Gas Reference from Atmospheric Carbon Dioxide Dry Air Mole Fractions from the NOAA ESRL Carbon Cycle Cooperative Global Air Sampling Network, available at: ftp://aftp.cmdl.noaa.gov/data/trace_gases/co2/flask/surface/ (last access: 27 July 2014), 2014.

Donlon, C. J., Nightingale, P. D., Sheasby, T., Turner, J., Robinson, I. S., and Emery, J.: Implications of the oceanic thermal skin temperature deviation at high wind speeds, Geophys. Res. Lett., 26, 2505–2508, 1999.

Donlon, C. J., Minnett, P., Gentemann, C., Nightingale, T. J., Barton, I. J., Ward, B., and Murray, J.: Towards improved validation of satellite sea surface skin temperature measurements for climate research, J. Climate, 15, 353–369, 2002.

Donlon, C., Robinson, I., Casey, K. S., Vazquez-Cuervo, J., Armstrong, E., Arino, O., Gentemann, C., May, D., Leborgne, P., Piollé, J., Barton, I., Beggs, H., Poulter, D. J. S., Merchant, C. J., Bingham, A., Heinz, S., Harris, A., Wick, G., Emery, B., Minnett, P., Evans, R., Llewellyn-Jones, D., Mutlow, C., Reynolds, R. W., Kawamura, H., and Rayner, N.: The GODAE High Resolution Sea Surface Temperature Pilot Project (GHRSST-PP), B. Am. Meteorol. Soc., 88, 1197–1213, 2007.

OSD
11, 1895–1948, 2014

Emery, W. J., Cherkauer, K., Shannon, B., and Reynolds, R. W.: Hull-mounted sea surface temperatures from ships of opportunity, J. Atmos. Ocean. Tech., 14, 1237–1251, doi:10.1175/1520-0426(1997)014<1237:HMSSTF>2.0.CO;2, 1997.

Emery, W. J., Baldwin, D. J., Schlüssel, P., and Reynolds, R. W.: Accuracy of in situ sea surface temperatures used to calibrate infrared satellite measurements, J. Geophys. Res., 106, 2387–2405, doi:10.1029/2000JC000246, 2001.

Fangohr, S. and Woolf, D. K.: Application of new parameterization of gas transfer velocity and their impact on regional and global marine CO_2 budgets, J. Marine Syst., 66, 195–203, 2007.

Jeffery, C. D., Woolf, D. K., Robinson, I. S., and Donlon, C. J.: One-dimensional modelling of convective CO_2 exchange in the Tropical Atlantic, Ocean Model., 19, 161–182, 2007.

Jeffery, C. D., Robinson, I., Woolf, D. K., and Donlon, C. J.: The response to phase-dependent wind stress and cloud fraction of the diurnal cycle of SST and air–sea CO_2 exchange, Ocean Model., 23, 33–48, 2008.

Kawai, Y. and Wada, A.: Diurnal sea surface temperature variation and its impact on the atmosphere and ocean: a review, J. Oceanogr., 63, 721–744, 2007.

Kennedy, J. J.: A review of uncertainty in in situ measurements and data sets of sea surface temperature, Rev. Geophys., 51, 1–32, doi:10.1002/2013RG000434, 2013.

Kennedy, J. J., Rayner, N. A., Smith, R. O., Saunby, M., and Parker, D. E.: Reassessing biases and other uncertainties in sea-surface temperature observations since 1850 Part 1: Measurement and sampling errors, J. Geophys. Res., 116, D14103, doi:10.1029/2010JD015218, 2011a.

Kennedy, J. J., Rayner, N. A., Smith, R. O., Saunby, M., and Parker, D. E.: Reassessing biases and other uncertainties in sea-surface temperature observations since 1850 Part 2: Biases and homogenisation, J. Geophys. Res., 116, D14104, doi:10.1029/2010JD015220, 2011b.

Kent, E. C., Taylor, P. K., Truscott, B. S., and Hopkins, J. A.: The accuracy of voluntary observing ship's meteorological observations, J. Atmos. Ocean. Tech., 10, 591–608, 1993.

Kettle, H. and Merchant, C. J.: Systematic errors in global air-sea CO_2 flux caused by temporal averaging of sea-level pressure, Atmos. Chem. Phys., 5, 1459–1466, doi:10.5194/acp-5-1459-2005, 2005.

Kettle, H., Merchant, C. J., Jeffery, C. D., Filipiak, M. J., and Gentemann, C. L.: The impact of diurnal variability in sea surface temperature on the central Atlantic air-sea CO_2 flux, Atmos. Chem. Phys., 9, 529–541, doi:10.5194/acp-9-529-2009, 2009.

OSD
11, 1895–1948, 2014

Land, P. E., Shutler, J. D., Cowling, R. D., Woolf, D. K., Walker, P., Findlay, H. S., Upstill-Goddard, R. C., and Donlon, C. J.: Climate change impacts on sea–air fluxes of CO_2 in three Arctic seas: a sensitivity study using Earth observation, Biogeosciences, 10, 8109–8128, doi:10.5194/bg-10-8109-2013, 2013.

Liss, P. S. and Merlivat, L.: Air-sea gas exchange rates: introduction and synthesis, in: The Role of Air–Sea Exchange in Geochemical Cycling, edited by: Buat-Menard, P., D Reidel, 113–127, 1986.

McKinley, G. A., Fay, A. R., Takahashi, T. and Metzl, N.: Convergence of atmospheric and North Atlantic carbon dioxide trends on multidecadal timescales, Nat Geosci., 4, 606–619, doi:10.1038/NGEO1193, 2011.

Merchant, C. J., Llewellyn-Jones, D., Saunders, R. W., Rayner, N. A., Kent, E. C., Old, C. P., Berry, D., Birks, A. R., Blackmore, T. , Corlett, G. K., Embury, O., Jay, V. L., Kennedy, J., Mutlow, C. T., Nightingale, T. J., O'Carroll, A. G., Pritchard, M. J., Remedios, J. J., and Tett, S.: Deriving a sea surface temperature record suitable for climate change research from the along-track scanning radiometers, Adv. Space Res., 41, 1–11, 2008.

Merchant, C. M., Embury, O., Rayner, N. A., David, I., Berry, D. I., Corlett, G. K., Lean, K., Veal, K. L., Kent, E. C., Llewellyn-Jones, D. T., Remedios, J. J., and Saunders, R.: A 20 year independent record of sea surface temperature for climate from Along-Track Scanning Radiometers, J. Geophys. Res., 117, C12013, doi:10.1029/2012JC008400, 2012.

O'Carroll, A. G., Eyre, J. R., and Saunders, R. W.: Three-way error analysis between AATSR, AMSR-E, and in situ sea surface temperature observations, J. Atmos. Ocean. Tech., 25, 1197–1207, doi:10.1175/2007JTECHO542.1, 2008.

Olsen, A., Omar, A. M., Stuart-Menteth, A. C., and Trinanes, J. A.: Diurnal variations of surface ocean pCO_2 and sea-air CO_2 flux evaluated using remotely sensed data, Geophys. Res. Lett., 31, L20304, doi:10.1029/2004GL020583, 2004.

Pebesma, E. J.: Gstat's User Manual, available at: http://www.gstat.org/gstat.pdf (last access: 27 February 2013), 1–100, 1999.

Pfeil, B. and Olsen, A.: A uniform format surface fCO_2 database, available at: http://www.socat.info/publications.html (last access: 4 June 2012), 1–9, 2009.

Pfeil, B., Olsen, A., Bakker, D. C. E., Hankin, S., Koyuk, H., Kozyr, A., Malczyk, J., Manke, A., Metzl, N., Sabine, C. L., Akl, J., Alin, S. R., Bates, N., Bellerby, R. G. J., Borges, A., Boutin, J., Brown, P. J., Cai, W.-J., Chavez, F. P., Chen, A., Cosca, C., Fassbender, A. J., Feely, R. A., González-Dávila, M., Goyet, C., Hales, B., Hardman-Mountford, N., Heinze, C., Hood, M.,

OSD
11, 1895–1948, 2014

Hoppema, M., Hunt, C. W., Hydes, D., Ishii, M., Johannessen, T., Jones, S. D., Key, R. M., Körtzinger, A., Landschützer, P., Lauvset, S. K., Lefèvre, N., Lenton, A., Lourantou, A., Merlivat, L., Midorikawa, T., Mintrop, L., Miyazaki, C., Murata, A., Nakadate, A., Nakano, Y., Nakaoka, S., Nojiri, Y., Omar, A. M., Padin, X. A., Park, G.-H., Paterson, K., Perez, F. F., Pierrot, D., Poisson, A., Ríos, A. F., Santana-Casiano, J. M., Salisbury, J., Sarma, V. V. S. S., Schlitzer, R., Schneider, B., Schuster, U., Sieger, R., Skjelvan, I., Steinhoff, T., Suzuki, T., Takahashi, T., Tedesco, K., Telszewski, M., Thomas, H., Tilbrook, B., Tjiputra, J., Vandemark, D., Veness, T., Wanninkhof, R., Watson, A. J., Weiss, R., Wong, C. S., and Yoshikawa-Inoue, H.: A uniform, quality controlled Surface Ocean CO_2 Atlas (SOCAT), Earth Syst. Sci. Data, 5, 125–143, doi:10.5194/essd-5-125-2013, 2013.

Reynolds, R. W., Gentemann, C. L., and Corlett, G. K.: Evaluation of AATSR and TMI satellite SST data, J. Climate, 23, 152–165, doi:10.1175/2009JCLI3252.1, 2010.

Sabine, C. L., Hankin, S., Koyuk, H., Bakker, D. C. E., Pfeil, B., Olsen, A., Metzl, N., Kozyr, A., Fassbender, A., Manke, A., Malczyk, J., Akl, J., Alin, S. R., Bellerby, R. G. J., Borges, A., Boutin, J., Brown, P. J., Cai, W.-J., Chavez, F. P., Chen, A., Cosca, C., Feely, R. A., González-Dávila, M., Goyet, C., Hardman-Mountford, N., Heinze, C., Hoppema, M., Hunt, C. W., Hydes, D., Ishii, M., Johannessen, T., Key, R. M., Körtzinger, A., Landschützer, P., Lauvset, S. K., Lefèvre, N., Lenton, A., Lourantou, A., Merlivat, L., Midorikawa, T., Mintrop, L., Miyazaki, C., Murata, A., Nakadate, A., Nakano, Y., Nakaoka, S., Nojiri, Y., Omar, A. M., Padin, X. A., Park, G.-H., Paterson, K., Perez, F. F., Pierrot, D., Poisson, A., Ríos, A. F., Salisbury, J., Santana-Casiano, J. M., Sarma, V. V. S. S., Schlitzer, R., Schneider, B., Schuster, U., Sieger, R., Skjelvan, I., Steinhoff, T., Suzuki, T., Takahashi, T., Tedesco, K., Telszewski, M., Thomas, H., Tilbrook, B., Vandemark, D., Veness, T., Watson, A. J., Weiss, R., Wong, C. S., and Yoshikawa-Inoue, H.: Surface Ocean CO_2 Atlas (SOCAT) gridded data products, Earth Syst. Sci. Data, 5, 145–153, doi:10.5194/essd-5-145-2013, 2013.

Takahashi, T., Sutherland, S. C., Sweeney, C., Poisson, A., Metzl, N., Tilbrook, B., Bates, N., Wanninkhof, R., Feely, R. A., Sabine, C., Olafsson, J., and Nojiri, Y.: Global air–sea CO_2 flux based on climatological surface ocean pCO_2, and seasonal biological and temperature effects, Deep-Sea Res. Pt. II, 45, 1601–1622, 2002.

Takahashi, T., Sutherland, S. C., Wanninkhof, R., Sweeney, C., Feely, R. A., Chipman, D. W., Hales, B., Friederich, G., Chavez, F., Sabine, C., Watson, A., Bakker, D. C. E., Schuster, U., Metzl, N., Yoshikawa-Inoue, H., Ishii, M., Midorikawa, T., Nojiri, Y., Körtzinger, A., Steinhoff, T., Hoppema, M., Olafson, J., Arnarson, T. S., Tilbrook, B., Johannesesen, T., Olsen, A.,

OSD
11, 1895–1948, 2014

Bellerby, R., Wong, C. S., Delile, B., Bates, N. R., and de Baar, H. J. W.: Climatological mean and decadal change in surface ocean pCO_2, and net sea–air CO_2 flux over the global oceans, Deep-Sea Res. Pt. II, 56, 554–577, 2009.

Takahashi, T., Sutherland, S. C., Chipman, D. W., Goddard, J. G., and Ho, C.: Climatological distributions of pH, pCO_2, total CO_2, alkalinity, and $CaCO_3$ saturation in the global surface Ocean, and temporal changes at selected locations, Mar. Chem., 164, 95–125, doi:10.1016/j.marchem.2014.06.004, 2014.

Wanninkhof, R., Asher, W. E., Ho, D. T., Sweeney, C., and McGillis, W. R.: Advances in quantifying air–sea gas exchange and environmental forcing, Annu. Rev. Mar. Sci., 1, 213–44, doi:10.1146/annurev.marine.010908.163742, 2009.

Ward, B., Wanninkhof, R., McGillis, W. R., Jessup, A. T., DeGrandpre, M. D., Hare, J. E., and Edson, J. B.: Biases in the air–sea flux of CO_2 resulting from ocean surface temperature gradients, J. Geophys. Res., 109, C08S08, doi:10.1029/2003JC001800, 2004.

Weiss, R. F.: Carbon dioxide in water and seawater: the solubility of a non-ideal gas, Mar. Chem., 2, 203–215, 1974.

Wilmott, C. J., Ackleson, S. G., Davis, R. E., Feddema, J. J., Klink, K. M., Legates, D. R., O'Donnell, J., and Rowe, C.: Statistics for the evaluation and comparison of models, J. Geophys. Res., 90, 8995–9005, 1985.

OSD
11, 1895–1948, 2014

Table 1. Differences between Takahashi climatology and climatology presented in this paper.

	Takahashi et al. (2009)	This study
Reference year	2000	2010
Resolution	$4^\circ \times 5^\circ$	$1^\circ \times 1^\circ$
Data	Excludes El Niño and coastal data	Includes El Niño and coastal data
Spatial Interpolation	Involves continuity equation based on a 2-D diffusion–advection transport equation for surface waters	Simple block kriging without continuity equation
Parameter	p_{CO_2} ($= f_{CO_2}$)	f_{CO_2} (and p_{CO_2})
f_{CO_2} taken at	instantaneous intake temperature SST_{depth}	monthly composite sub skin SST from ARC

OSD
11, 1895–1948, 2014

Table 2. The different kriging options that were applied to the monthly data sets of $f_{CO_2,cl}$ for 2010; ordinary block kriging was applied with min, max, radius, dx and dy as explained in Sect. 4.

min	max	radius	dx	dy
4	20	60	5	5
4	20	40	5	5
4	20	100	5	5
4	20	60	1	1
4	20	60	10	10
4	10	60	5	5
4	40	60	5	5
2	20	60	5	5
10	20	60	5	5

OSD
11, 1895–1948, 2014

Table 3. Error estimations of the parameters involved in the $f_{CO_2,cl}$ computation and their consequent errors $\Delta f_{CO_2,cl}$ (µatm).

Parameter x	error	$\Delta f_{CO_2,cl}$
ΔSST	±0.05*	±0.75
ΔT_{eq}	±0.05*	±0.015
ΔP_{eq}	±0.5*	∼ 0
$\Delta f_{CO_2,is}$	±2*	±2
$\Delta T_{ym,i}$	±0.2	±3

* for SOP data (Pfeil et al., 2013).

OSD
11, 1895–1948, 2014

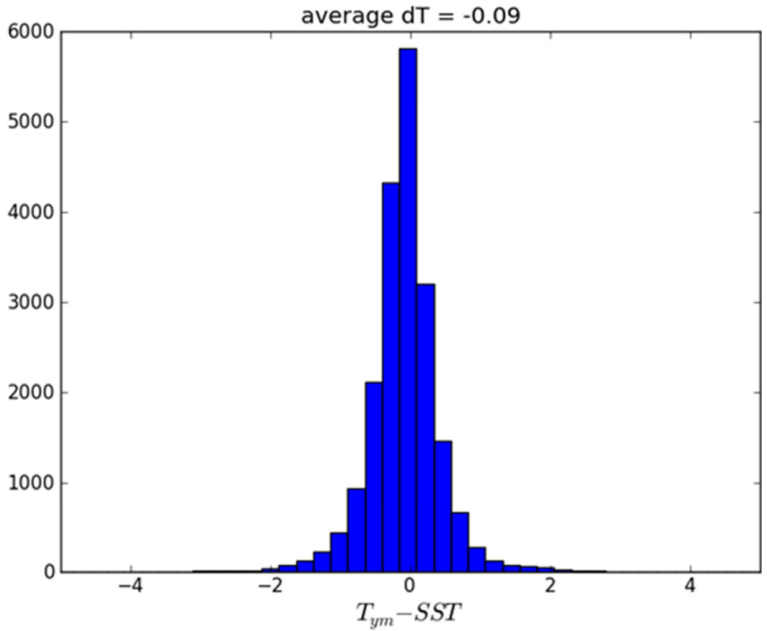

Figure 1. Histogram of temperature difference between monthly gridded data of subskin SST derived from ARC, T_{ym}, and in situ SST from SOCAT version 1.5 using global data from all available years.

OSD
11, 1895–1948, 2014

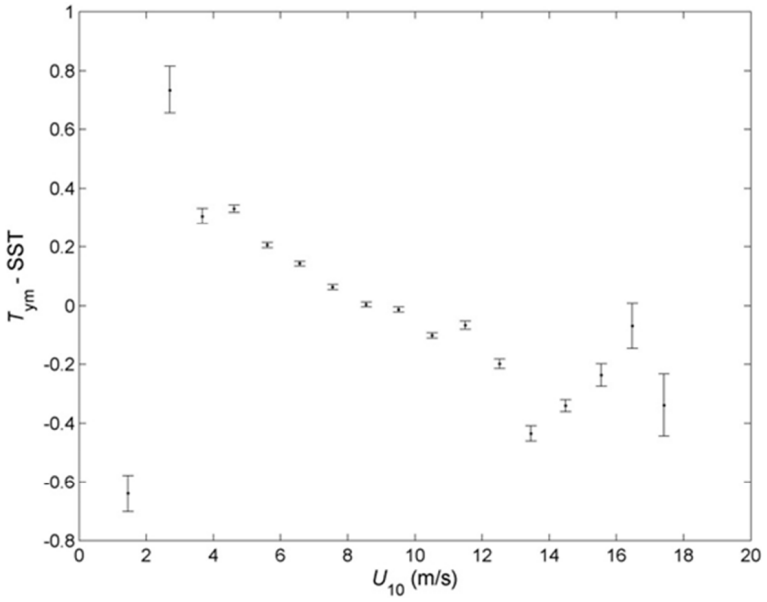

Figure 2. Scatter plot of temperature difference between monthly gridded data of subskin SST derived from ARC, T_{ym}, and in situ SST from SOCAT version 1.5, using data from all available years in the North Atlantic, binned in 1 m s^{-1} U_{10} bins. The error bar indicates the standard error of the mean.

OSD
11, 1895–1948, 2014

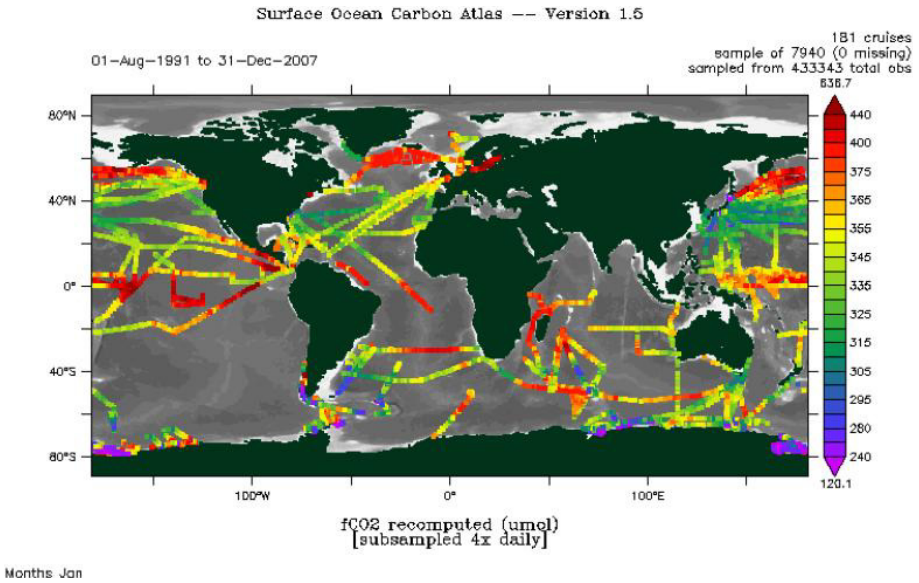

Figure 3. SOCAT CO_2 fugacity (µatm) data shown in the online Cruise Data Viewer for the month January; all data from 1 August 1991 to 31 December 2007.

OSD
11, 1895–1948, 2014

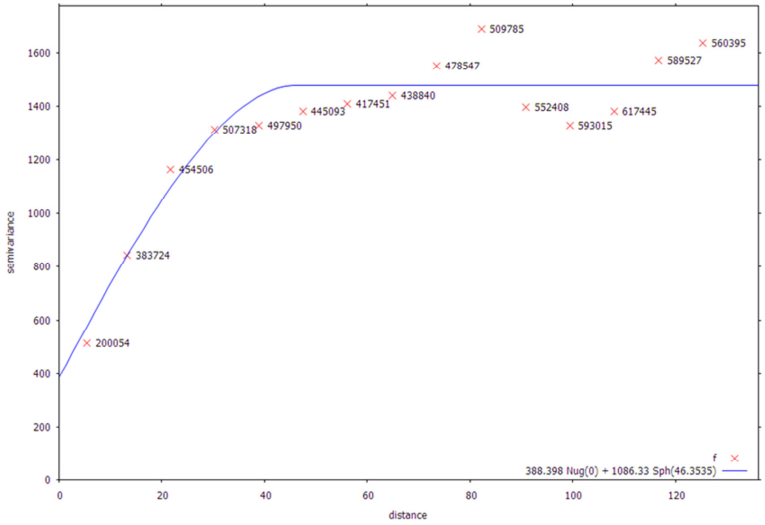

Figure 4. Variogram for global $f_{CO_2,cl}$ data in 2010 for the month January, derived from $f_{CO_2,is}$ shown in Fig. 3. The numbers next to each data point are the number of data pairs.

OSD
11, 1895–1948, 2014

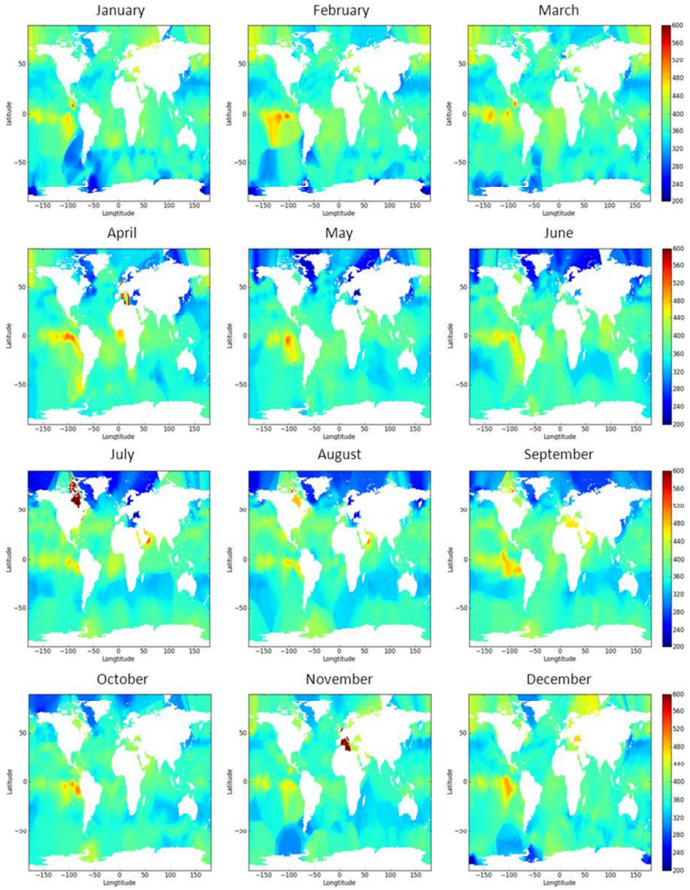

Figure 5. Monthly $f_{CO_2,cl}$ values in the global oceans estimated for 2010 for January (top left) to December (bottom right) on a 200–600 µatm scale; data were interpolated to a 1° × 1° grid using ordinary block kriging with min = 4, max = 20, radius = 60 and block size 5 × 5.

OSD
11, 1895–1948, 2014

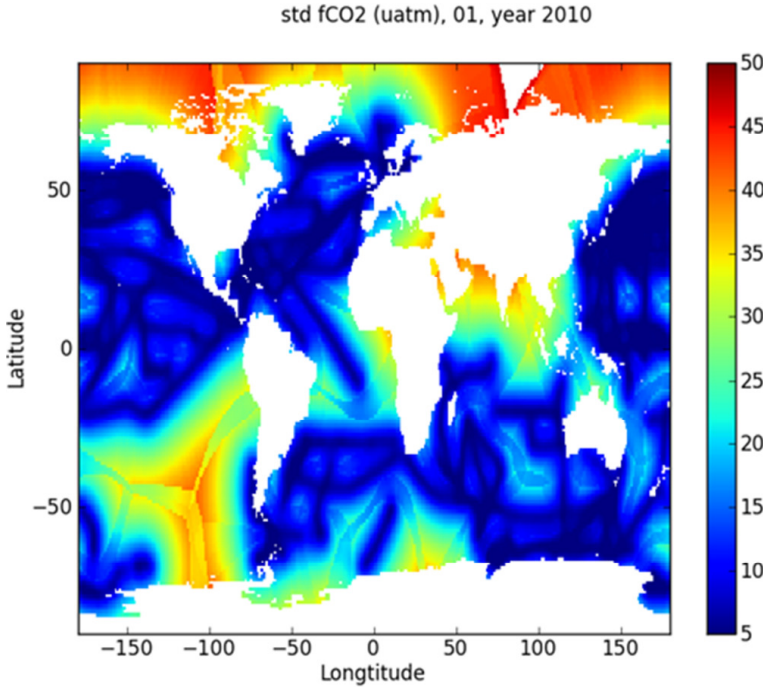

Figure 6. Standard deviation in $f_{CO_2,cl}$ estimated for January 2010 on a 5 to 50 µatm scale, associated with the ordinary block kriging shown in Fig. 5.

OSD
11, 1895–1948, 2014

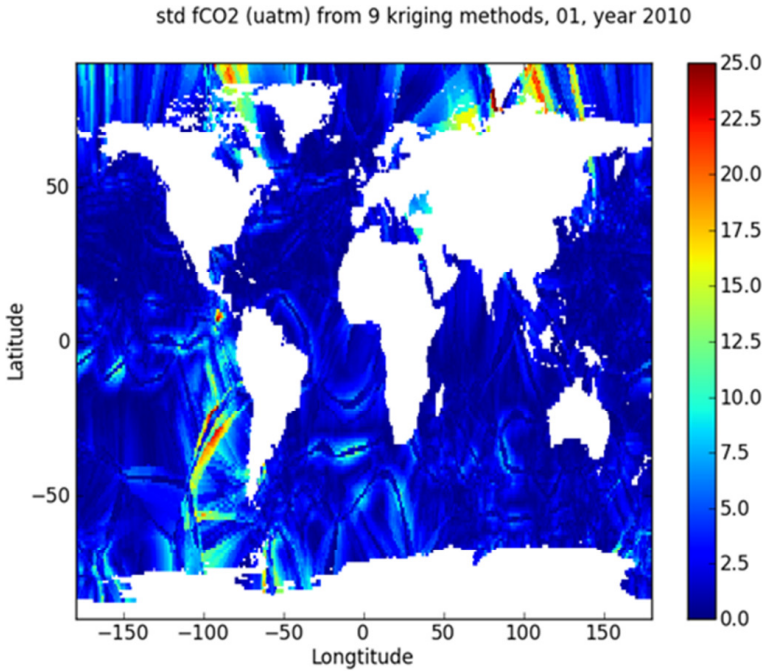

Figure 7. Standard deviations of the mean over nine different kriging results of $f_{CO_2,cl}$ estimated for January 2010, using the range of options shown in Table 2; on a 0 to 25 µatm scale.

OSD
11, 1895–1948, 2014

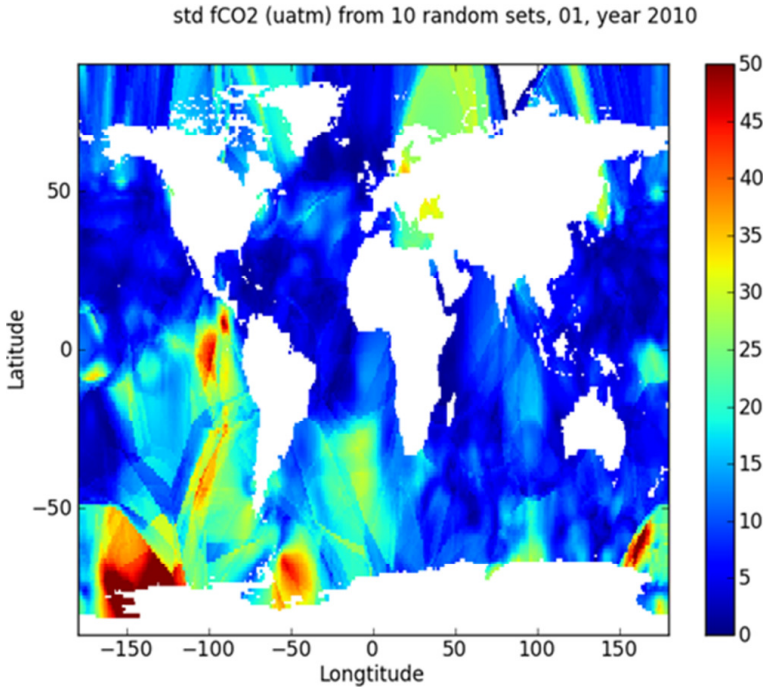

Figure 8. Standard deviations of the mean over 10 bootstrapped datasets of $f_{CO_2,cl}$ estimated for January 2010; on a 0 to 50 µatm scale.

OSD
11, 1895–1948, 2014

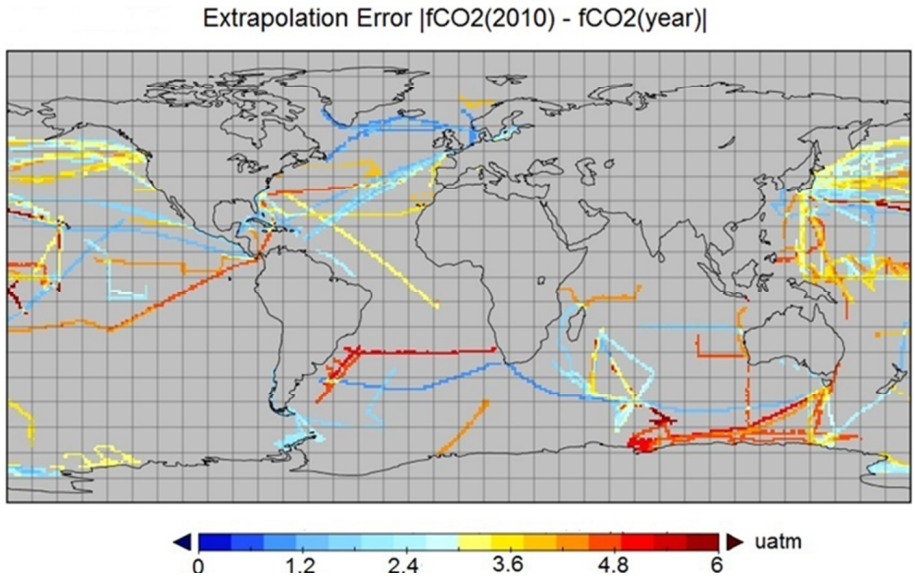

Figure 9. Calculated propagation of the "temporal extrapolation error" in $f_{CO_2,cl}$ estimated for January 2010 due to uncertainty in p_{CO_2} trend; on a 0 to 6 µatm scale.

OSD
11, 1895–1948, 2014

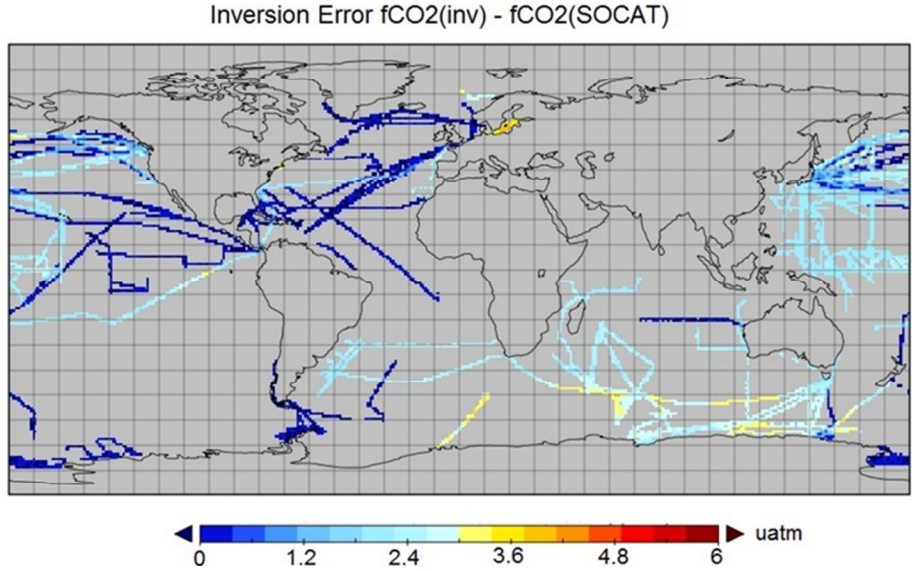

Figure 10. Calculated "inversion error" in $f_{CO_2,cl}$ estimated for January 2010, on a 0 to 6 µatm scale.

OSD
11, 1895–1948, 2014

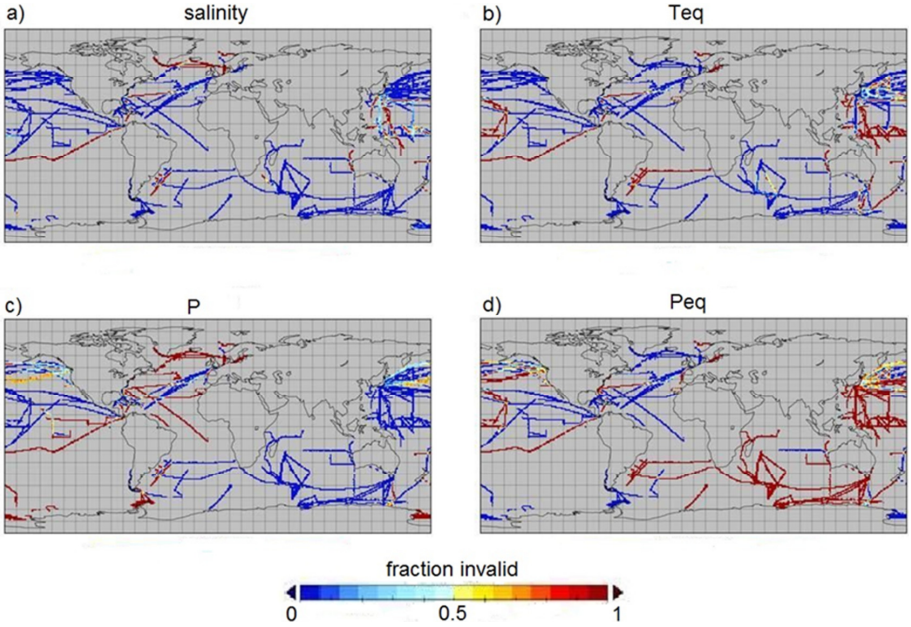

Figure 11. Fractions of $f_{CO_2,cl}$ estimated for January 2010, calculated with missing value **(a)** salinity, **(b)** T_{eq}, **(c)** P, and **(d)** P_{eq}; on a 0 to 1 scale.

OSD
11, 1895–1948, 2014

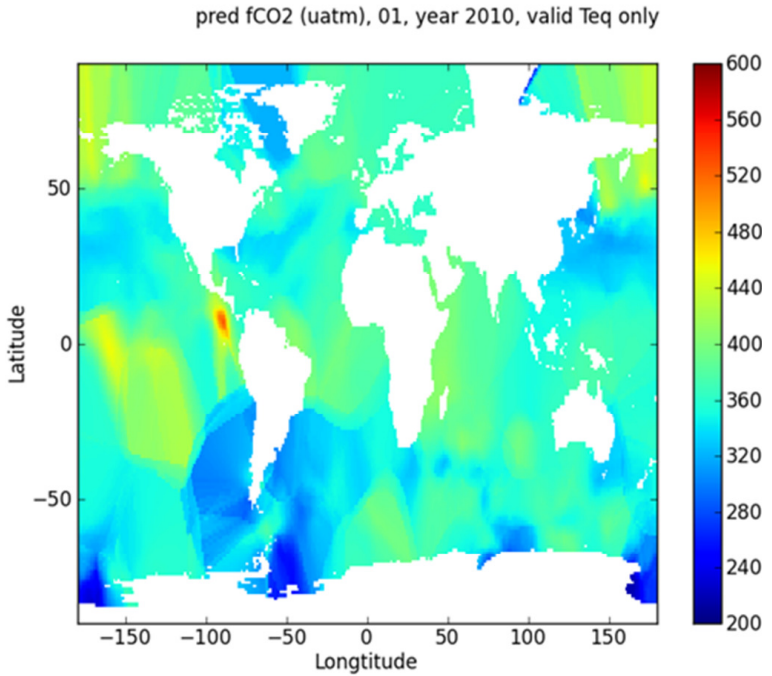

Figure 12. As Fig. 5, January, but using only data points with valid T_{eq}.

OSD
11, 1895–1948, 2014

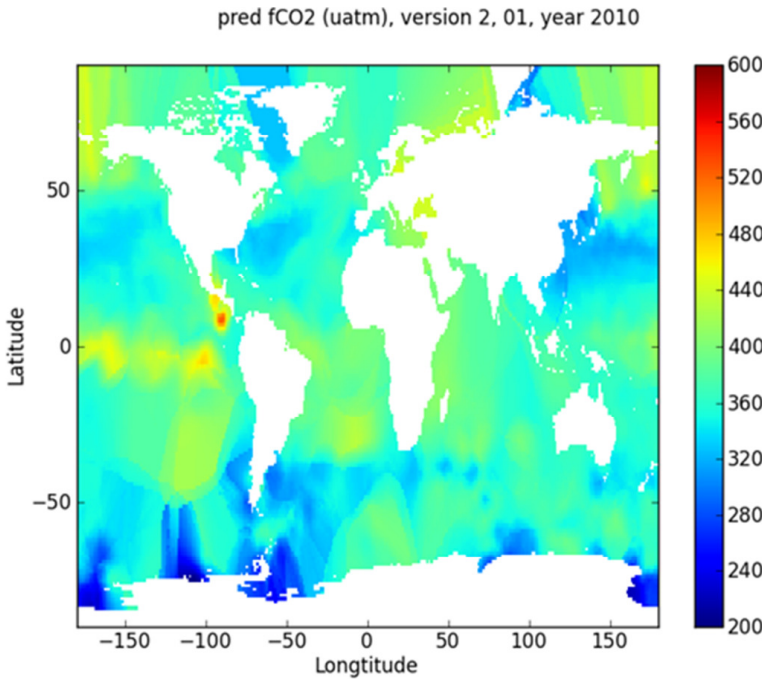

Figure 13. As Fig. 5, January, but using SOCAT version 2 data.

OSD
11, 1895–1948, 2014

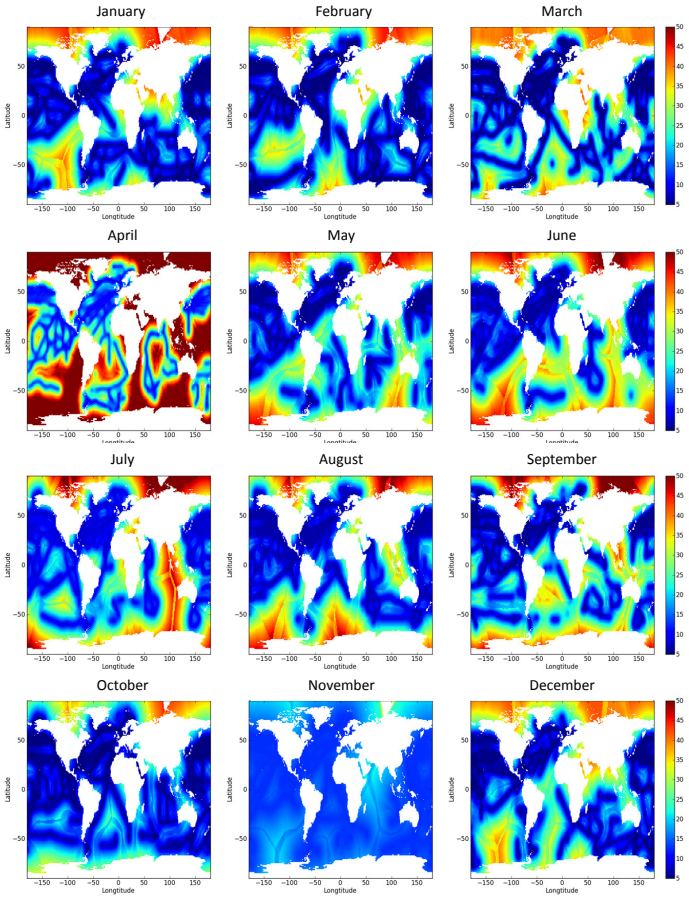

Figure A1. Spatial interpolation errors in estimations of $f_{CO_2,cl}$ in 2010. Standard deviation in $f_{CO_2,cl}$ estimated for 2010 associated with the ordinary block kriging results shown in Fig. 5; on a 5 to 50 µatm scale.

OSD
11, 1895–1948, 2014

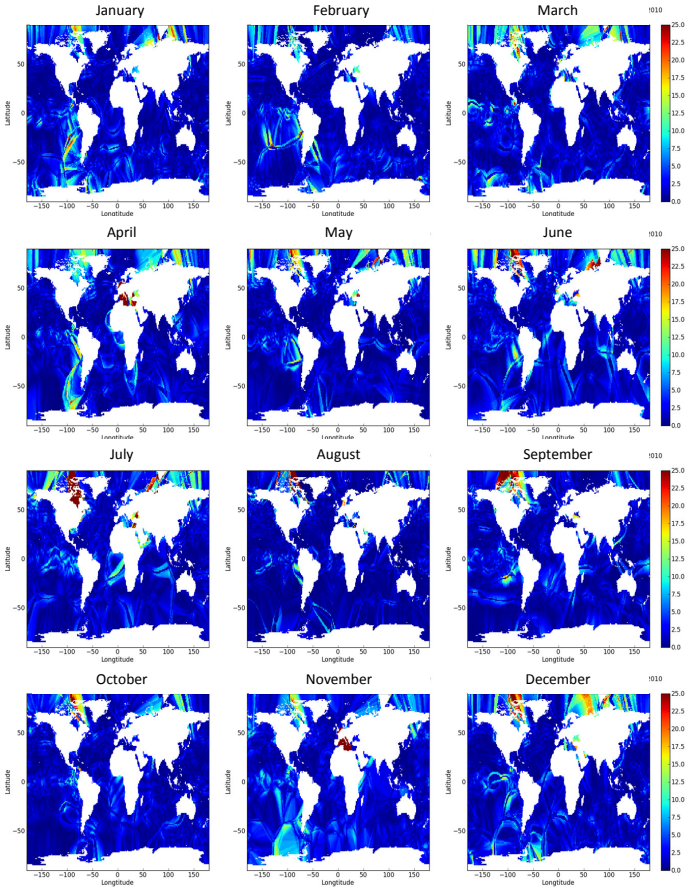

Figure A2. Variation in $f_{CO_2,cl}$ in 2010 distributions due to different kriging approaches. Standard deviations of the mean over the different kriging results of $f_{CO_2,cl}$ estimated for 2010, using the range of options shown in Table 1; on a 0 to 25 µatm scale.

OSD
11, 1895–1948, 2014

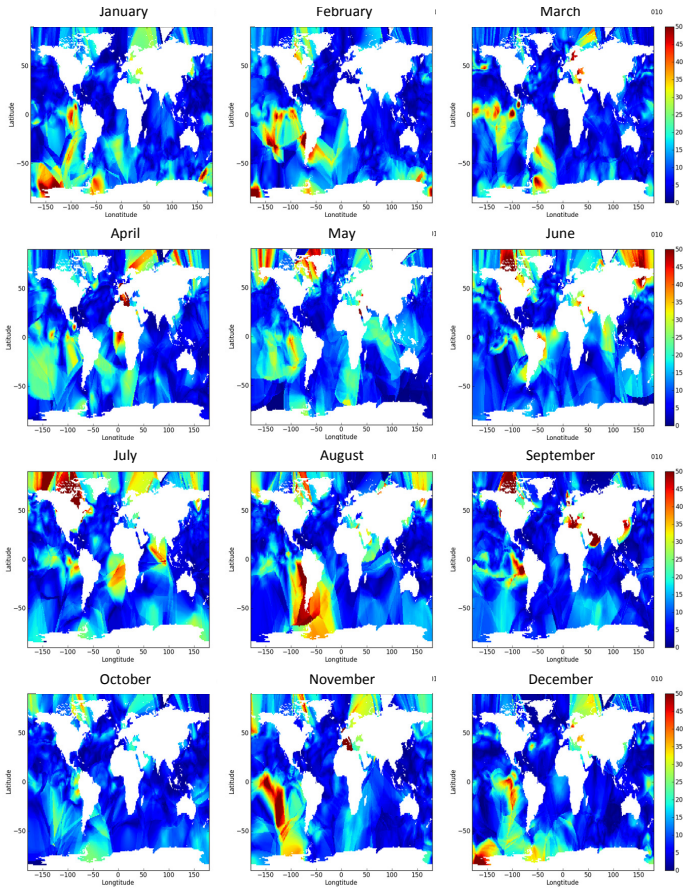

Figure A3. Errors in $f_{CO_2,cl}$ in 2010 by bootstrapping cruises. Standard deviations of the mean over 10 bootstrapped datasets of $f_{CO_2,cl}$ estimated 2010; on a 0 to 50 µatm scale.

OSD
11, 1895–1948, 2014

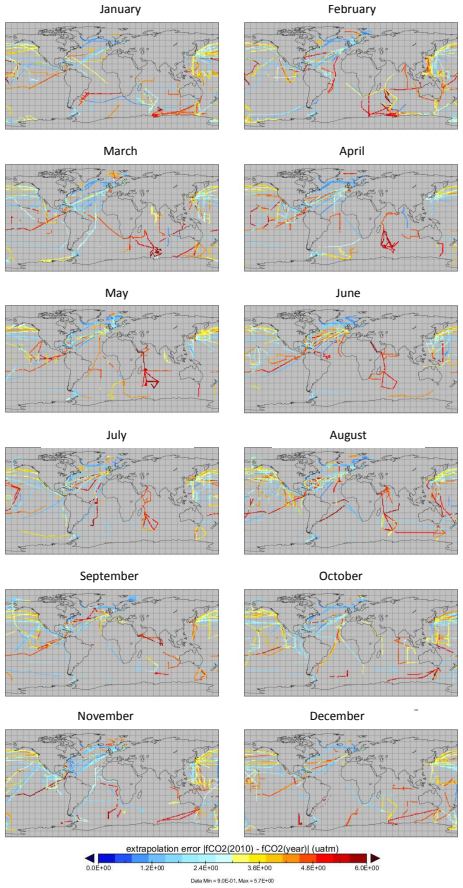

Figure A4. Estimated errors in $f_{CO_2,cl}$ in 2010 due to the extrapolation to the year 2010. Calculated propagation of the "temporal extrapolation error" in $f_{CO_2,cl}$ estimated for 2010 due to uncertainty in p_{CO_2} trend, on a 0 to 6 µatm scale.

OSD
11, 1895–1948, 2014

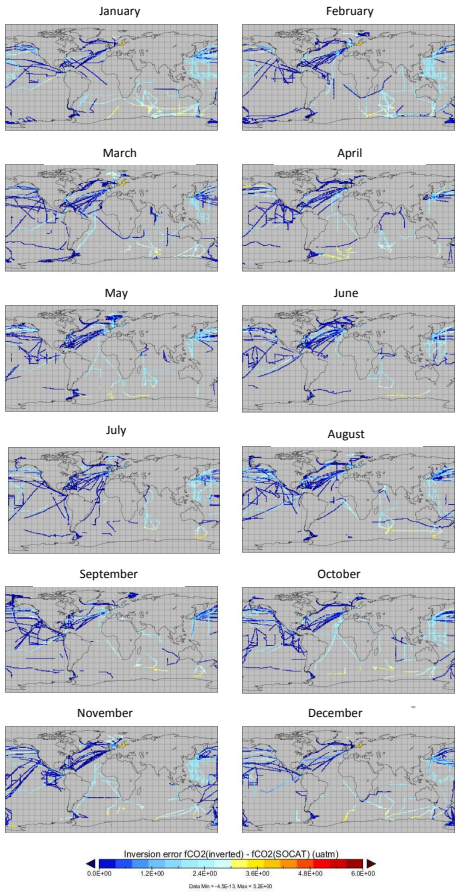

Figure A5. Estimated errors in $f_{CO_2,cl}$ in 2010 due to the inversion step. Calculated propagation of the "inversion error" in $f_{CO_2,cl}$ estimated for 2010, on a 0 to 6 µatm scale.

OSD
11, 1895–1948, 2014

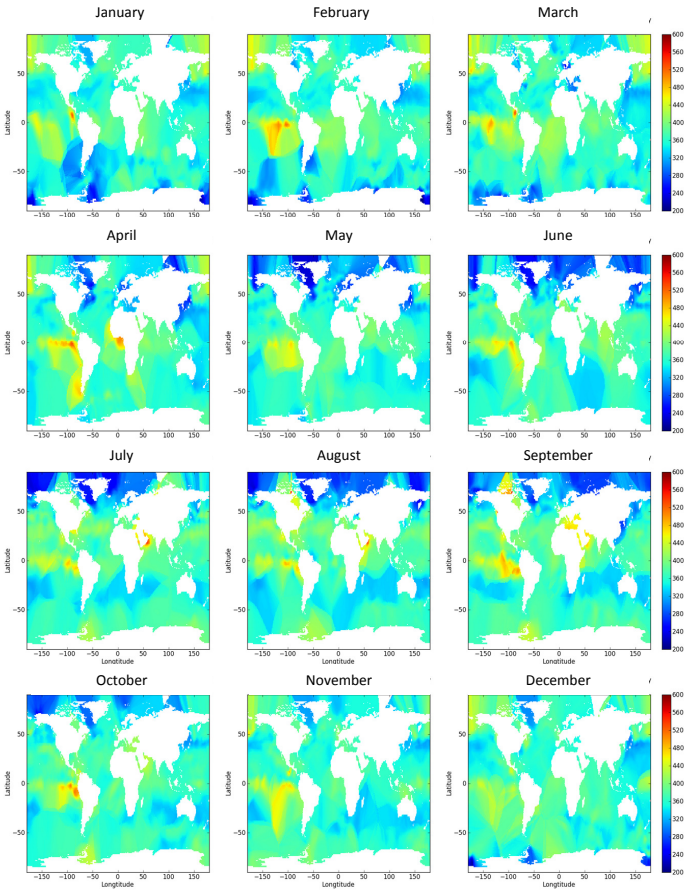

Figure A6. Monthly global distributions of $f_{CO_2,cl}$ in 2010, using data points with T_{eq} only. As Fig. 5, but for data points with valid T_{eq} values only.

OSD
11, 1895–1948, 2014

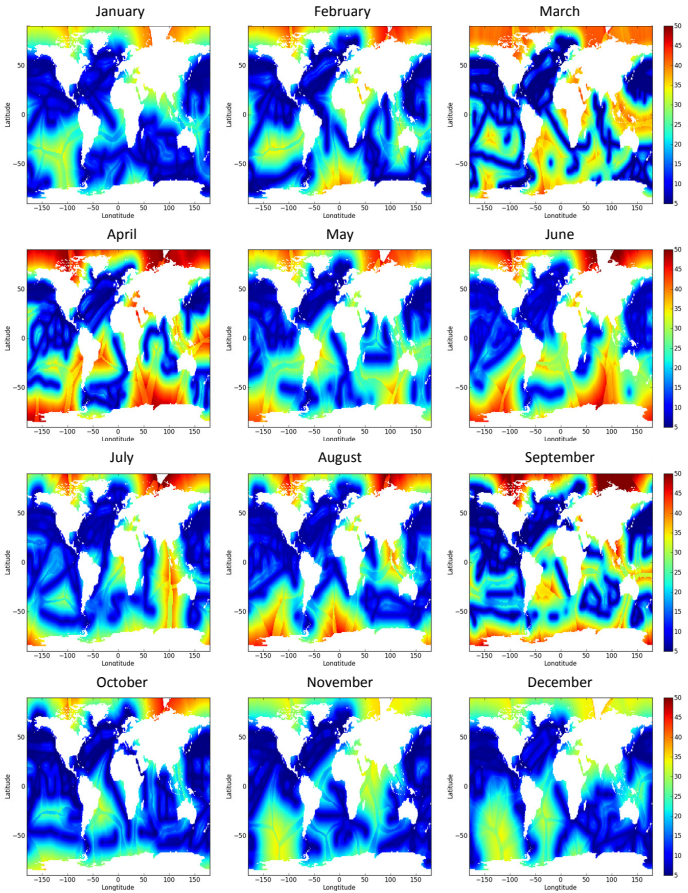

Figure A7. Spatial interpolation errors in estimations of $f_{CO_2,cl}$ in 2010, using data points with T_{eq} only. As Fig. A1, but for data points with valid T_{eq} values only.

OSD
11, 1895–1948, 2014

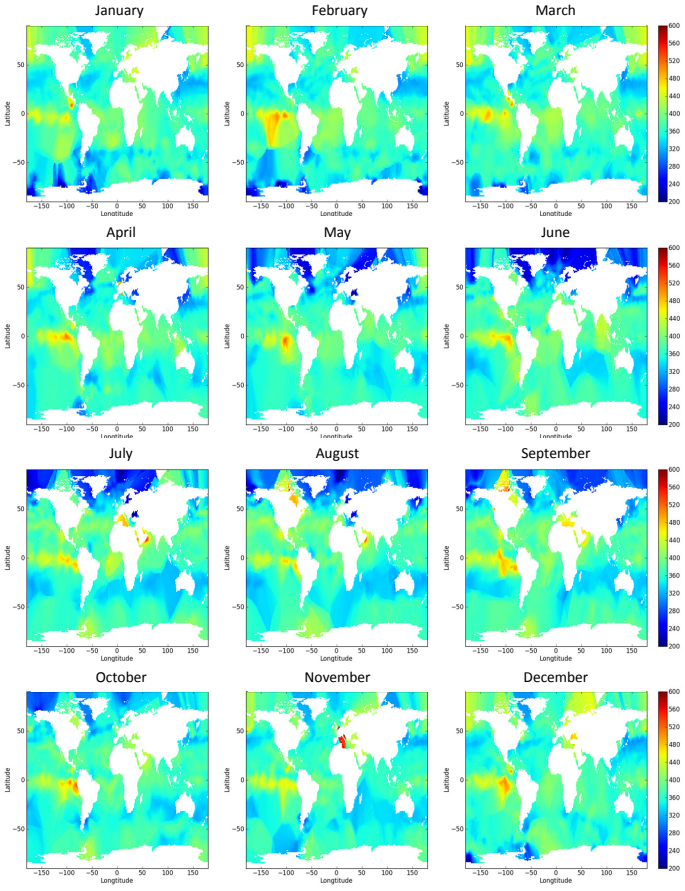

Figure A8. Monthly global distributions of $f_{CO_2,cl}$ in 2010 from SOCAT version 2. As Fig. 5, but for SOCAT version 2 instead of version 1.5.

OSD
11, 1895–1948, 2014

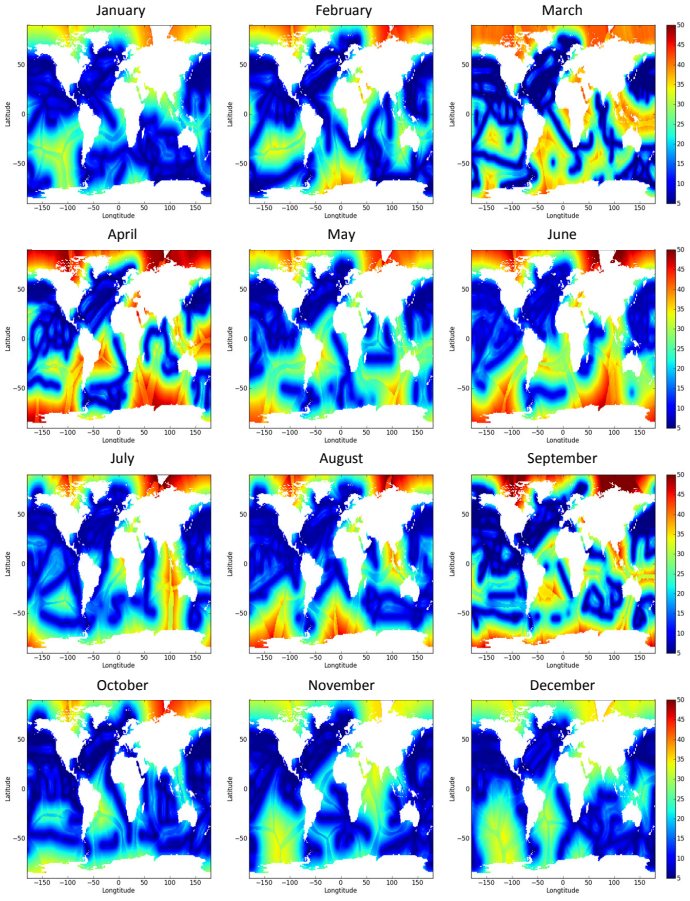

Figure A9. Spatial interpolation errors in $f_{CO_2,cl}$ in 2010 using SOCAT version 2. As Fig. A1, but for SOCAT version 2 instead of version 1.5.

OSD
11, 1895–1948, 2014